EFFECT OF SMALL AMOUNT OF ALUMINIUM ON THE STRUCTURE AND PROPERTIES OF HYPOEUTECTOID STEEL

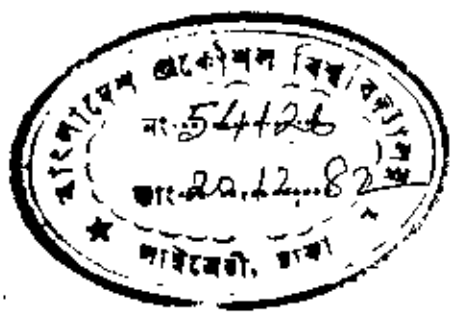

BANGLADESH UNIVERSITY of ENGINEERING & TECHNOLOGY
Dhaka.

EFFECT OF SMALL AMOUNT OF ALUMINIUM ON THE STRUCTURE AND PROPERTIES OF HYPOEUTECTOID STEEL

A thesis submitted to the Department of Metallurgical Engineering, BANGLADESH UNIVERSITY of ENGINEERING & TECHNOLOGY, Dhaka, in partial fulfillment of the requirements for the degree of Master of Science in Engineering (Metallurgical).

Sayeeduddin Mahmood

November, 1982

BANGLADESH UNIVERSITY of ENGINEERING & TECHNOLOGY

C E R T I F I C A T E

This is to certify that this work has been carried out by the author under the joint supervision of Dr. Ehsanul Haque, Associate Professor, and Dr. M. M. A. Bepari, Assistant Professor, Department of Metallurgical Engineering, BANGLADESH UNIVERSITY of ENGINEERING & TECHNOLOGY, Dhaka, and it has not been submitted anywhere else for the award of any other degree or diploma.

E. Haque
Supervisor

Author

Md. Mohar Ali Bepari
Co-supervisor

Accepted as satisfactory for partial fulfillment of the requirements for the degree of Master of Science in Engineering (Metallurgical).

E. Haque

Dr. Ehsanul Haque, Associate Professor,
Department of Metallurgical Engineering,
BUET, Dhaka. — Chairman (Supervisor)

Md. Mohar Ali Bepari

Dr. M.A. Bepari, Assistant Profeesor,
Department of Metallurgical Engineering,
BUET, Dhaka. — Member (Co-Supervisor)

Dr. S. Islam, Professor and Head,
Department of Metallurgical Engineering,
BUET, Dhaka. — Member

Nooruddin ahmed

Dr. Nooruddin Ahmed, Professor,
Department of Chemical Engineering,
BUET, Dhaka. — Member

Dr. Alimullah Khan, Managing Director,
Prokaushali Sangsad,
Dhaka. — Member (External)

ACKNOWLEDGEMENTS

The author is deeply indebted to, and expresses his gratitude to Dr. Ehsanul Haque and Dr. M. M. A. Bepari, Department of Metallurgical Engineering, BANGLADESH UNIVERSITY of ENGINEERING & TECHNOLOGY, for their guidance and encouragement in all stages of the project as well as in preparing the thesis.

The author is grateful to Dr. M. Ibrahim, Professor, and Dr. Serajul Islam, Professor and Head, Department of Metallurgical Engineering, BANGLADESH UNIVERSITY of ENGINEERING & TECHNOLOGY, for their inspiration and help in all aspects of the project.

The author would like to thank all concerned in the Bangladesh Atomic Energy Commission, specially Mr. A. Mazid, Head, Technical Physics Division, for their inspiration which helped in completion of the requirements for the degree.

Special acknowledgements must be made to the help provided by all the staff concerned of the BANGLADESH UNIVERSITY of ENGINEERING & TECHNOLOGY, who helped in different stages of this project.

ABSTRACT

(3A)

The relationship of the mechanical properties with composition and structural parameters is an important consideration in the metallurgical design of ferritic-pearlitic steels. In this project the effect of aluminium on the properties of hypocutectoid steel has been studied.

The austenite grain coarsening behaviour of the steels was first investigated. The isothermal transformation technique used, revealed the prior austenite grain boundaries satisfactorily in the plain carbon steel. In the aluminium alloyed steel, the presence of aluminium together with high manganese, carbon and silicon was observed to retard the rejection of ferrite when held at inter-critical temperatures. The variation of prior austenite grain size with temperature indicated that aluminium nitride was effective in austenite grain refinement upto 1050°C. Above this temperature the grain coarsening was rapid in aluminium alloyed steel.

The standard tensile and charpy V-notch specimens of the steels were heat-treated at temperatures corresponding to a common austenite grain size and cooled at four different cooling rates. The ferrite grain size after transformation was measured by the mean linear intercept method. It was found that carbon, manganese and soluble aluminium caused ferrite grain refinement and increased the yield strength. Aluminium, either as aluminium nitride or dissolved in ferrite raised the impact transition temperature. Increasing carbon also increased the impact transition temperature.

CONTENTS

Chapters		Page
1	Introduction	1
2	High Strength Low Alloy Structural Steels	2
2.1	Requirements	2
2.2	Development of HSLA Steels	2
2.3	Factors Affecting Strength and Toughness of HSLA Steels	3
2.3.1	Ferrite Grain Size	3
2.3.2	Precipitation Strengthening	10
2.3.3	Solid Solution Strengthening	17
2.3.3.1	Dislocation Locking	18
2.3.3.2	Dislocation Friction	21
2.4	Solubility Product and Stoichiometric Ratio	24
2.5	Metallurgical Design of Ferrite-Pearlite Steels	26
3.	Experimental Procedures	29.
3.1	Materials and Specimen Preparation	29
3.2	Measurement of Prior Austenite Grains	30
3.2.1	Isothermal Transformation Technique	30
3.3	Determination of Heat-Treatment Temperature	31
3.4	Heat-Treatment of Specimens	31
3.5	Mechanical Testing of Tensile and Charpy V-notch Specimens	33
3.5.1	Tensile Test	33
3.5.2	Charpy V-notch Test	34
3.6	Determination of Ferrite Grain Size and Hall-Petch Plots	34
4	Experimental Results	36
4.1	Prior Austenite Grain Size	36
4.2	Heat Treatment Temperature	36
4.3	Optical Microscopy	37
4.4	Ferrite Grain Size and Hall-Petch Plots	37
4.5	Impact Test	37

Chapters		Page
5	Discussion	64
5.1	Making of Aluminium-Alloyed Steel	64
5.2	Prior Austenite Grain Size	65
5.2.1	Isothermal Transformation Technique	65
5.2.2	Effect of Precipitates on the Prior Austenite Grain Size	67
5.3	Ferrite Grain Size and Hall-Petch Plots	67
5.4	Impact Transition Temperature	70
6	Conclusion and Future Suggestions	73
6.1	Conclusions	73
6.2	Future Suggestions	74
	References	

Chapter 1

INTRODUCTION

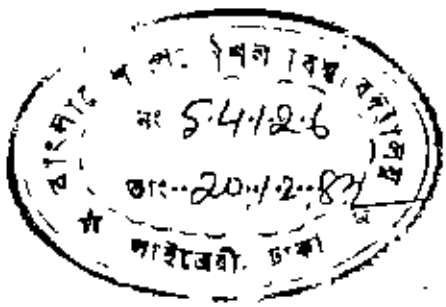

① Low alloy strengthening is quite dd. Certain of V SS
② Def. of microalloy

Chapter 1

INTRODUCTION

This thesis work is an attempt to study the low alloy strengthening effect of the steel produced in the Chittagong Steel Mills Ltd., (CSM). This low alloy strengthening process has been developed quite recently. In the advanced countries it has become possible to double the yield strength of structural steels with micro-alloy addition and proper heat-treatment. This might prove a tremendous economic benefit for Bangladesh.

A comparative study of properties of ordinary CSM) steel and aluminium-alloyed steel (with proper treatment) was made. The steel-alloy was produced in the Departmental induction furnace. It was then rolled from a local re-rolling mill.

To relate the structure and properties and to understand the effect of micro-alloy addition, structural changes had to be determined. The prior austenite grain size which greatly influences the subsequent ferrite grain size were determined by Isothermal Transformation Technique (Phillips & Chapman, 1963) rather than by the recently developed oxidation technique (Niltawach, 1977) due to lack of experimental facilities.

The effect of micro-alloy addition needed to be analysed by electron microscopy and also X-ray diffraction. However, in the absence of these vital instruments analysis were made on the basis of optical microscopy and mechanical test results with the help of theoretical presumptions.

Chapter 2

HIGH STRENGTH LOW ALLOY STRUCTURAL STEELS

Chapter 2

HIGH STRENGTH LOW ALLOY (HSLA) STRUCTURAL STEELS

2.1 Requirements

Properties required of structural steels in present day engineering design, for the fabrication of steel structures, pressure vessels, ships etc. may be summarized as follows:

i. High yield strengths, greater load-bearing capacities for lighter sections.
ii. High toughness, i.e. low Impact Transition Temperature and high Ductile Shelf Energy.
iii. High ductility level and fracture resistance in the through thickness direction.
iv. High index of weldability.
v. Good formability especially in bending.

Ferrite and pearlite are the main micro-constituents of structural steels. However, acicular structures such as bainite and low carbon matrensite are useful when high yield strengths are to be obtained.

2.2 Development of HSLA Steels

Previously the design of HSLA steels was based on tensile strength, with little importance being attached to weldability, formability and resistance to brittle fracture. Carbon was

Is carbon an alloying element?

used as an alloying element to obtain tensile strengths required. These steels though of the ferrite-pearlite type were relatively high in carbon percentage (over 0.3%).

With the introduction of welding, structural failures resulted which required an improvement in toughness and weldability. It was found that better weldability and lower impact transition temperature (ITT) was obtained by decreasing the carbon content (Barr, 1950). Also a high yield strength was found to be more important than a high tensile strength.

Hall (1951) and Petch(1953, 1959) demonstrated that ferrite grain refinement increases the yield strength and decreases the impact transition temperature. Grain refining was done with aluminium and nitrogen through the formation of aluminium nitride precipitates (Wiester & Ulmer, 1959). Later other additives such as vanadium and niobium were found to produce grain refinement by precipitation of vanadium and niobium carbonitrides. Development of the methodology of structure-property relationships (Pickering & Gladman, 1963) hastened the introduction of normalised grain refined steels. Later it was found that the precipitation of niobium or vanadium carbides additionally strengthened the steel, over and above that resulting from the fine grain size (Morrison & Woodhead, 1963).

2.3 Factors Affecting Strength and Toughness of HSLA Steels

2.3.1 Ferrite Grain Size

Increase of yield strength and decrease of impact transition temperature is greatly dependent on the ferrite grain size. Quantitative relationship between microstructural and compositional parameters and the mechanical properties of silicon killed, carbon-manganese steels have been summarized

by Pickering (1975) in two equations:

$$\text{Yield stress } (N/mm^2) = 54 + 32\ (\%\ Mn) + 83\ (\%\ Si) + 355\ (\sqrt{\%N_f}) + 17.4\ (d^{-\frac{1}{2}}) \quad \ldots(2.1)$$

$$\text{Impact Transition Temperature } (^{o}C) = -19 + 44\ (\%\ Si) + 700\ (\sqrt{\%\ N_f}) + 2.2\ (\%\ \text{pearlite}) - 11.5\ (d^{-\frac{1}{2}}) \quad \ldots(2.2)$$

where 'N_f' is free nitrogen and 'd' is the ferrite grain size.

From these equations it is evident that a small ferrite grain size is important in improving both yield strength and toughness. Increase in Carbon content, i.e. pearlite, reduces the Charpy Upper Shelf Energy (Gladman et al, 1972) and has a detrimental effect on the Impact Transition Temperature. A low carbon content is necessary to form the finest possible grain size.

Models of grain control have been proposed by Zener, Paranjpe, Hillert, Webster and Gladman. These were reviewed by S.Niltawach (1977) and Bepari (1981). The present review summarizes Gladman's (1966) theory in the light of ferrite grain control.

Refining the prior-austenite grain size is the pre-requisite for fine ferrite grains because ferrite grains nucleate on the austenite grain boundaries. Austenite grain growth is inhibited by micro alloying additions of suitable materials which result in the presence of second phase particles in the austenite. The interaction of these particles

with the austenite grain boundaries affects the grain coarsening behaviour of austenite. Smith (1948) has shown that this interaction results from the reduction of grain boundary area when the boundary intersects the second phase particles. Any movement of the grain boundary away from the particle would cause an increase in energy and have a drag effect on the migrating boundary. McLean (1957) has shown that the binding force between the particle and boundary is greater than that available by thermal activation. Thus energy for unpinning must come from other sources, such as the energy release resulting from grain growth.

Zener (1949) related the size of spherical grains 'R' with the size of spherical precipitate particles 'r'. By analogy with surface tension force he showed that the maximum force 'B' exerted by a particle or boundary would be

$$B = \pi r \gamma \quad \ldots\ldots\ldots (2.3)$$

where γ is the surface energy per unit area of boundary.

Assuming the driving force for grain growth to be $2\gamma / R_o$, Zener's ultimate criterion is

$$R = \frac{4}{3} r/f \quad \ldots\ldots\ldots (2.4)$$

where f is the volume fraction of precipitate particles.

This model has however been shown to be overestimated.

Hillert (1965) has related the growth of metal grains and the energy changes involved by a simple method of the energy change, E, where

$$-E = K (1/R_c - 1/R) \quad \ldots\ldots\ldots\ldots (2.5)$$

where R is the radius of any grain and R_c is the critical radius.

Grains larger than critical size would cause a decrease in energy whereas smaller grains cause an increase in energy.

Gladman (1966) explored the effect of precipitate particles on grain growth in metals by development of a theoretical model.

The physical model (Gladman, 1966) for pinning of a boundary by a spherical particle is shown in Fig. 1. The pinning mechanism is largely due to reduction in grain boundary area when a grain boundary intersects a particle. The lowest energy position of the boundary when it contact a single particle will occur when the boundary intersects a particle across a diameteral plane.

Values of the energy change acompanying both flexible and rigid boundary motion away from the diameteral position are shown in the form of a normalized graph. Fig. 2.

Energy changes accompanying a migration of a pinned boundary have shown that the criterion for unpinning can be expressed as:

$$r^* = \frac{6 R_o f}{\pi} \left(\frac{3}{2} - \frac{2}{Z} \right) \quad \ldots\ldots\ldots\ldots (2.6)$$

The critical particle radius r* can then be calculated from a knowledge of the volume fraction of the particles f, the matrix grain radius R_o, and the ratio of the radius of the larger grain to that of its neighbours, Z.

For most polygonal structures a Z value of 1.5 is reasonably suggested by experimental work. In equation 2.6 the critical particle radius increases as either the

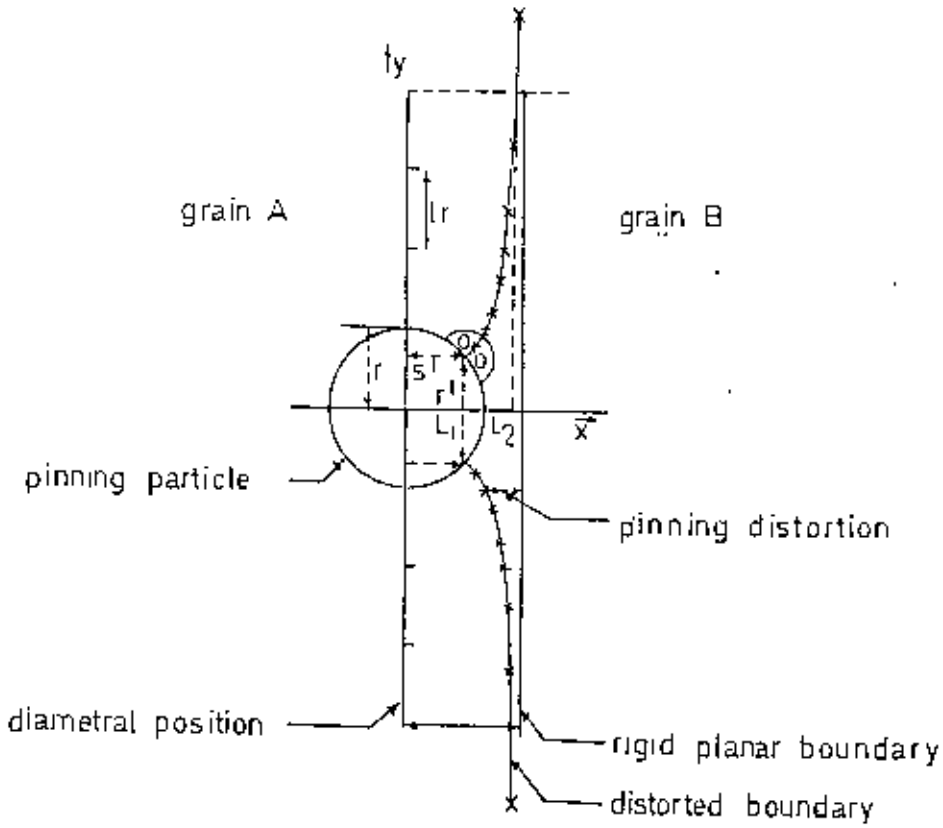

Fig. 1. Model for unpinning.

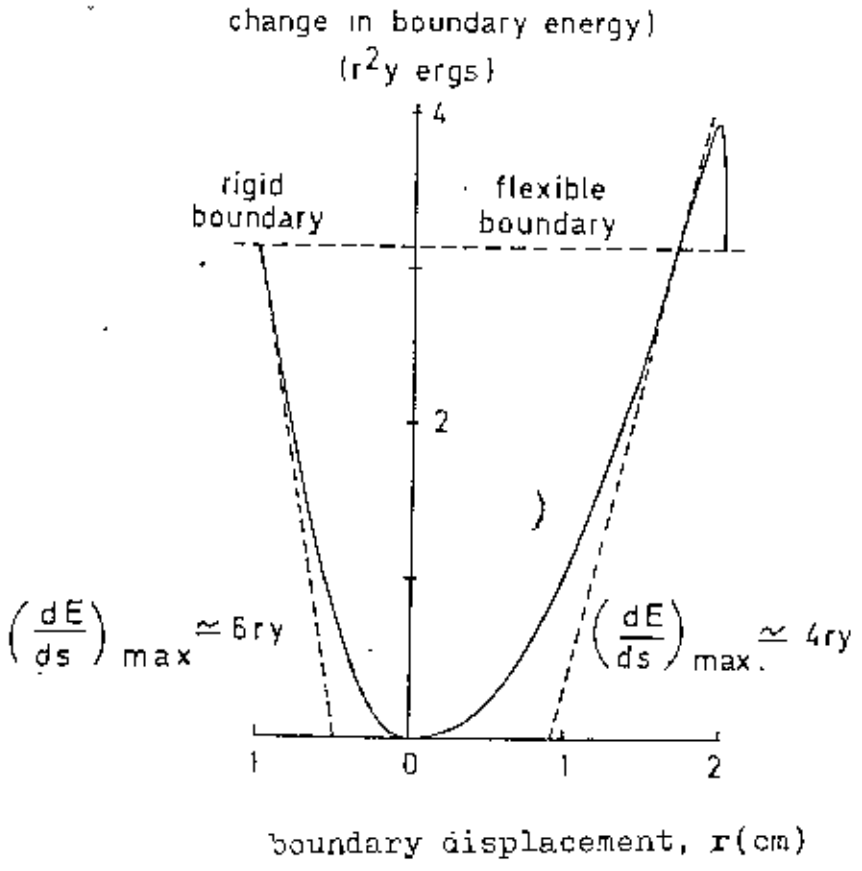

Fig. 2 Energy change due to unpinning.

volume fraction of particles or the matrix grain size increases. Increase of grain size hetrogenity decreases the critical particle radius. At some critical particle size, the driving force for grain growth equals the pinning force. If the particle radius increase further, the driving force exceeds the pinning force. Thus fine particles are more effective than coarse particles in restricting grain growth.

In the normalized condition, austenite grain refinement is achieved by pinning with precipitates of aluminium nitride or the carbonitrides of niobium, vanadium and titanium. Bepari and Woodhead (1982) reported that on heating, vanadium carbonitride is much more effective in austenite grain refinement than vanadium carbide at all temperatures. The effect of vanadium carbonitride, in austenite grain refinement is more or less the same as that of aluminium nitride at temperatures below 1000°C but this effect decreases with increasing temperature, and above 1000°C aluminium nitride is a much better grain refiner than vanadium carbonitride. They also reported that the precipitating particles of vanadium carbide and particularly vanadium carbonitrides are excellect ferrite grain refiners while aluminium has little or no effect in ferrite grain size refinement. For effective pinning, the specific alloy addition must be selected to produce fine particles. A fine initial particle size is desirable to prolong the time taken for the particle to reach the critical particle size above which grain growth occurs. The ferrite grain size achieved by this method is $\sim 5\,\mu m$. Depressing the transformation temperature, either by alloy additions or by increasing the cooling rate, is also used to give grain refinement provided acicular structures are not produced. Controlled rolling techniques also give very fine grain size, possibly somewhat smaller than $\sim 5\,\mu m$.

2.3.2 Precipitation Strengthening

The formation of a precipitate greatly strengthens an alloy. The increase in yield stress depends principally on the strength, structure, spacing, size, shape and distribution of the precipitate particles as well as on the degree of misfit or coherency with the matrix and on their relative orientation.

In steels the addition of small amounts of other metals have the effect of strengthening the ferrite matrix by formation of fine precipitates. The effectiveness of precipitation strengthening from alloy addition depends upon the solubility in austenite of the precipitating phase and its precipitation kinetics during cooling. Titanium, niobium, vanadium and aluminium are important alloy additions for precipitation strengthening. The strength rises mainly from the precipitation of nitrides, carbides and carbonitrides. It has been established that aluminium precipitates as aluminium nitride. It has been reported by Bepari (1981) that vanadium carbide and vanadium carbonitrides are excellent precipitation strengtheners while aluminium nitride does not produce any appreciable precipitation strengthening effect.

W.C.Leslie et al (1953) has shown that the formation of aluminium nitride follows the well known pattern of precipitation from super-saturated solid solution, in that the rate of formation is low at high temperature (925°C), increases to a maximum at intermediate temperature (815°C), and then rapidly decreases with decreasing temperature (705° & 545°C). The aluminium nitride content increases with time at the holding temperature upto a maximum characteristic of each temperature.

Carbides and nitrides present in a matrix mean that they hinder the movement of migrating dislocations. A dislocation moving on its slip plane containing a distribution of precipitate particles may cut through the particles or avoid them by moving out of its slip plane or by bending between the particles, leaving a dislocation ring around each precipitate particle. For a dislocation to shear a particle sufficient energy must be supplied to break favourable bonds within the particle thus increasing its surface area (Kelly & Nicholson, 1963) Fig. 3.

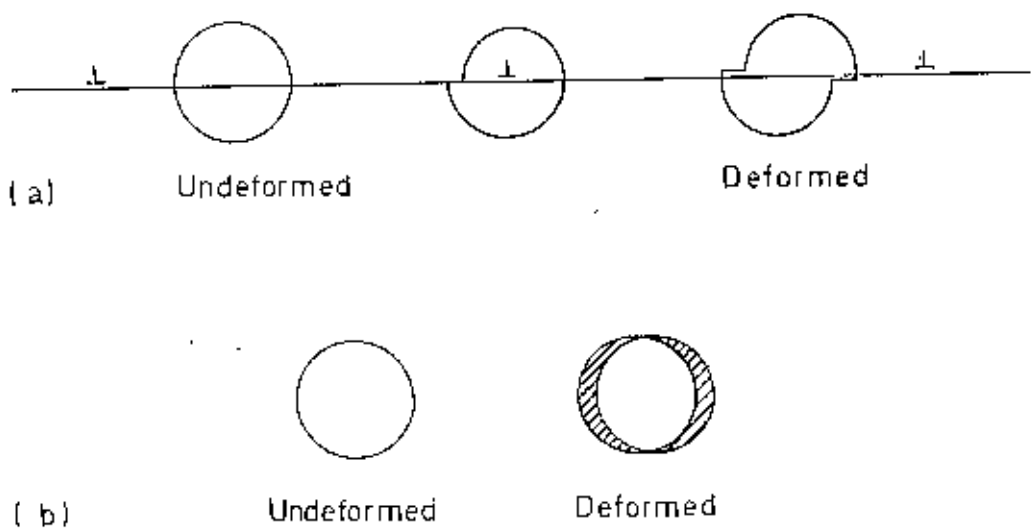

Fig. 3. A dislocation moves from left to right through a precipitate which cuts its slip-plane, producing an increase in the area of the matrix - precipitate. (a) View in the slip-plane normal to the Burgers vector of the dislocation. (b) View normal to the slip-plane.

The maximum precipitation hardening which results from competing shear and Orowan mechanisms is therefore reached in the ferrite and micro-alloy precipitate systems as soon as very small precipitates occur with diameters of only a few lattice constants.

Three basic approaches have been made to the problem of yielding in crystals containing a dispersed phase. The first considers the long range interactions between particles and the dislocations in the matrix irrespective of whether, during plastic flow, the particles are sheared by the dislocations or not. The second considers yielding by the matrix dislocations gliding so that they avoid the particles, so that flow takes place without particle shear. The third considers the mechanism by which shearing of the particles takes place at yield.

The best known of theories describing the yield stress due to long-range interactions between dislocations and precipitates is that of Mott and Nabarro (1940) based on the consideration of the internal stresses arising when the average atomic volume in the matrix material is different from that in the precipitate. This stress is equated to the yield stress of the crystal.

The increase in yield stress due to precipitation strengthening arises principally from the direct interaction between dislocations and the distributed second-phase particles. Orowan (1948) explained the cause of the decrease of the yield stress when the critical particle size is exceeded. He showed that yield can occur without particle shear. To quantify this Orowan proposed the following model. Assuming the total volume of precipitates to be constant, large distances between the particles means large particle size and hence the presence of extensive regions of negative internal stress around the particles, which act as obstacles to advancing

dislocation lines. Driven by the externally applied stress, a moving dislocation line encountering second phase particles will be held back at the regions of high negative stress around the particles. It will bulge forward or bow into the gaps between the particles until it forms a semi-circular shape of which the diameter is approximately equal to the spacing between the two surfaces. As the applied stress increases,. the line bulges more strongly. The dislocation configuration then becomes unstable and segments of the dislocation line are constrained to form a dislocation loop around each particle. The main dislocation is thus free to continue its passage through the lattice,Fig. 4. As new dislocation lines come along, each repeats this process and leaves a new dislocation loop around the obstacles. The shear stress at an obstacle rises with the number of the encircling loops, and finally it is bound to overcome the resistance of the local internal stress, either by enforcing glide, or by tearing away the precipitated particle.

Orowan showed that the yield strength of the alloy is the sum of the matrix flow stress τ_m and the resolved shear stress to bow dislocations between the dispersed particles.

$$YS = \tau_m + \frac{2T}{bL} \qquad \ldots\ldots\ldots\ldots\ldots (2.7)$$

where T= line tension of dislocation,
b= burger's vector.

Explain ?

Consequently we see that the yield stress is approximately equal to the shear stress necessary for forcing a dislocation line through a row of obstacles of spacing L.

Kelly and Nicholson (1963) quantifying short-range interactions modified the Orowan equation. They used the approximation for the line tension of dislocation $T = \frac{1}{2}Gb^2$ to give the equation:

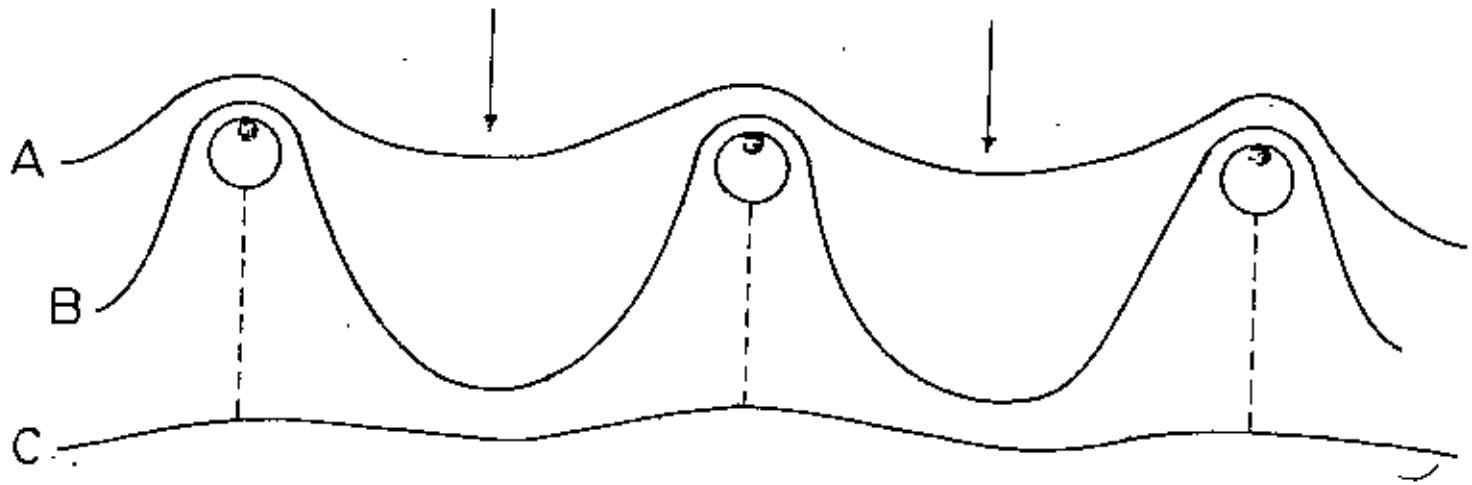

Fig. 4. Schematic representation of dislocations passing between widely spaced precipitates.

$$YS = \tau_m + \frac{Gb}{L} \quad \ldots\ldots\ldots\ldots\ldots (2.8)$$

where G = shear modulus of the matrix plane.

The Orowan bowing theory holds valid only when the dislocations are confined in their slip plane, the particles are neither sheared nor fractured in the bowing process and lastly the structural feature which controls the matrix flow stress, i.e. uniformly retards dislocation movement over distances which are large compared with the planar inter-particle spacing.

Ashby (1966) further refined the Orowan approach. He recalculated the line tension of dislocation taking into account the effects of the character of the dislocation, and scale of the bending and stacking fault or anti-phase boundary energy, thus proposing the most sucessful modification of the Orowan model. The only major difference between the two models is that the Ashby-Orowan model predicts that edge dislocations bypass particles more easily than do screw dislocations whereas the original Orowan model predicts the reverse.

The Ashby-Orowan model is considered feasible because it takes into account the Kocks (1966) model in which realistic random particle distribution is assumed. The Ashby-Orowan model can be expressed quantitatively as follows:

$$\tau = \frac{1}{1.18} \left(\frac{1.2\ Gb}{2\pi L} \right) \ln \left(\frac{X}{2b} \right) \quad \ldots\ldots\ldots (2.9)$$

where τ = the resolved shear stress in N/mm^2

X= mean planar intercept diameter of a precipitate

The values for G and b for ferrite, 80300 N/mm^2 and (2.5°A) respectively are substituted giving:

$$\tau = \frac{2.6}{L} \ln \left(\frac{X}{0.00025} \right) \quad \ldots\ldots\ldots\ldots\ldots (2.10)$$

Assuming that the yield stress increment due to particles is twice the resolved shear stress required to overcome their effect,

$$YS_p = \frac{5.2}{L} \ln \left(\frac{X}{0.00025} \right) \quad \ldots\ldots\ldots\ldots\ldots (2.11)$$

Assuming that the particles are spheroidal, their volume fraction can be given by:

$$f = n_s \left(\frac{\pi X^2}{4} \right)$$

where n_s is the number of particles per unit area of the slip plane.

Then

$$L = X \left(\sqrt{\frac{\pi}{4f}} - 1 \right)$$

For the relatively small fractions of fine precipitates formed in micro-alloyed steels,

$$L \gg X,$$

Then

$$L = X \left(\sqrt{\frac{\pi}{4f}} \right) \quad \ldots\ldots\ldots\ldots\ldots (2.12)$$

The final expression of the yield strength due to precipitates can then be written as :

$$YS_p = \frac{5.9 \sqrt{f}}{X} \ln \left(\frac{X}{0.00025} \right) \quad \ldots\ldots (2.13)$$

We see that the stress increment due to fine precipitates increases with the reduction in precipitate size and the increase in fine precipitate fraction. The close agreement between the observed increment associated with precipi-

tation strengthening and the increment predicted from the model implies that the increase in yield stress over that expected from grain size in the microalloyed steel is due entirely to the precipitation strengthening.

The cooling rate also controls the degree of precipitation. A rapid cooling rate supresses precipitation while a slow cooling rate allows the precipitate to overage. In between there is an intermediate cooling rate which optimises the precipitation strengthening.

2.3.3 Solid Solution Strengthening

A solid solution is obtained when atoms of different elements are able to share together and with changing proportions, various sites of a common crystalline lattice. All metals and compounds show some solubility in the solid state, however complete solid solubility can occur only if the structures of the elements involved are basically the same, but it need not occur when this condition is fulfilled.

From the point of view of solid solubility chemical compounds can be compared with pure metals and may be said to show alloying behaviour if they exhibit wide solid solubility in a phase diagram. Since compounds are usually formed at fixed ratios of atoms the occurence of solid solubility represents a departure from stochiometry.

In addition to the change of dislocation structure on alloying there are direct interactions between solute atoms and dislocations to be considered as mechanisms of solid solution hardening. These can be divided into two groups; Dislocation Locking; and Dislocation Friction.

2.3.3.1 Dislocation Locking

This is the case in which solute atoms collect on dislocations at rest. Here a pronounced yield point should be observed. Slip tends to concentrate by continuing where it started. The different mechanisms are briefly described with respect to their overall dependence on solute concentration 'c', and temperature of deformation 'T'.

(a) Chemical Locking Interaction

Suzuki (1957) observed that the stacking fault in an fcc lattice can be considered a hexagonal layer a few atoms thick. Solubility in this hexagonal "phase" may differ from that in the fcc matrix, and solute can thus segregate in the fault. Haque et al (1975) actually measured an extra atomic displacement due to stacking fault and also observed the concentration of point defects near the fault in HVEM. Edge dislocations and to a lesser extent screw dislocations thus become pinned. For a dislocation to break loose an extra stress must be applied which depends on concentration 'c'. The magnitude of $\Delta\tau_c$ depends upon the thermochemical parameters characterstic of the alloy (Cotrell, 1954; Flinn,1958). Typically

(b) Elastic Locking

Cotrell (1954) showed that atoms of different size substituted in a crystal produce localized elastic strain fields which interact with those of dislocations. Compensating for their respective distortions, foreign atoms of different size energetically occupy favourable positions near dislocations. The elastic interaction energy between an edge dislocation and a substitutional atom may amount to several-tenths of an electron volt. Since a screw dislocation has no hydrostatic stress field, its interaction with atoms of different size is much smaller. A stress increment $\Delta\tau_c$ is needed to initiate dislocation movement which depends on 'c' in a manner similar

to Suzuki interaction, $\Delta\tau_c$ is proportional to the misfit parameter:

$$\delta = \frac{1}{a}\frac{da}{dc}$$

where, 'a' is the lattice constant of the alloy.

Again, $\Delta\tau_c$ is independent of temperature except for the case when an, 'atmosphere' of foreign atoms 'condenses' along the dislocation core. Then $\Delta\tau_c$ should decrease with increasing T as T^{-3} (Haasen, 1959).

(c) Stress-Induced Order Locking, Schoeck - Snoek Effect

In this mechanism, the directionality of forces exerted by the dislocation on its environment may produce local order in the alloy around it. The dislocation "digs itself in" energetically in this way and a yield point may result. The effect should depend quadratically on concentration in the case of substitutional alloys. Schoeck and Seegar (1959) calculated it to be independent of temperature below the temperature of rapid diffusion. The effect acts differently on edge and screw dislocations.

A simple illustration of stress induced order is provided by the behaviour of interstitial atoms, notably carbon atoms in a b.c.c. lattice, Fig. 5. In absence of an external stress the interstitial atoms are distributed at random on the sites marked a, b and c. However if a tensile stress is applied along a crystal axis, the 'c' sites become favoured over others. An interstitial atom on a 'c' site distrorts the lattice in the same direction as does the external stress. The stress induces a certain amount of order in the lattice. The greater the stress, the higher the degree of order. This

effect may involve either interstitial or substitutional alloying atoms.

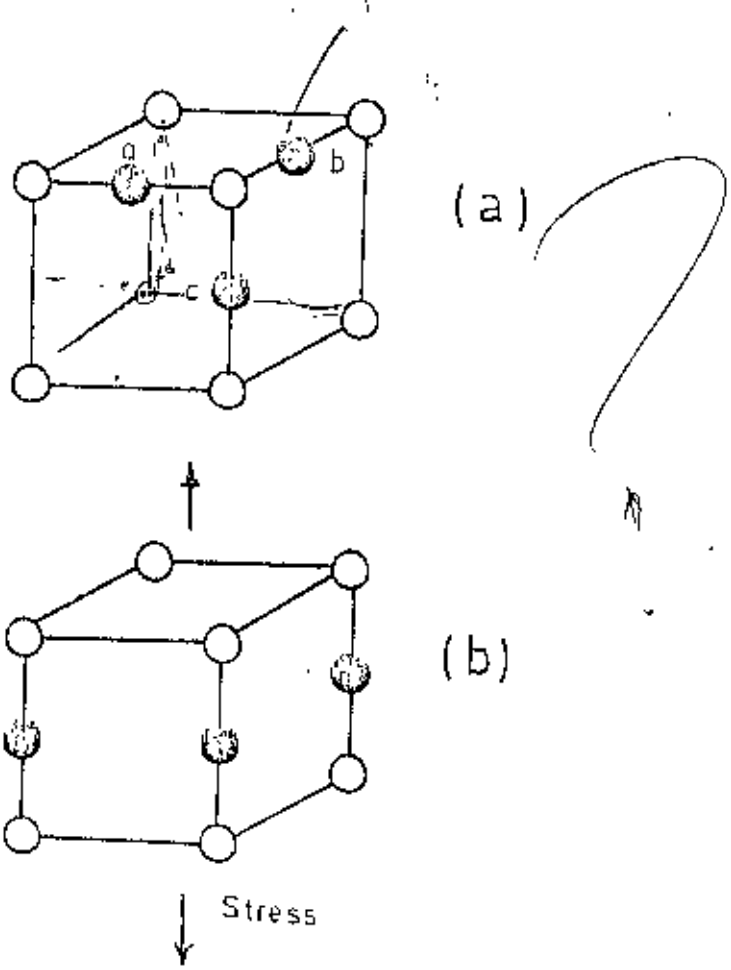

Fig. 5. Illustration of stress induced order of interstitial atoms in b.c.c. structure: (a) no stress (b) stress.

The ordering of the region around a dislocation reduces the total energy of the crystal. As a result the dislocation tends to be pinned to its site.

2.3.3.2 Dislocation Friction

In the case of dislocation friction the solute atoms act on moving dislocations. The effect of friction is simply to shift the whole stress/strain curve to higher stresses, although the friction may slowly decrease with increasing strain; a gradual yield point is then observed.

The friction mechanisms acting on freely moving dislocations are:

(a) Diffuse Forces

Matt and Naborro (1948) showed that solute atoms of size misfit δ in an alloy produce an internal stress field of volume average $\tau_i = \mu\delta c$. Its effect on a moving dislocation depends on the degree of dispersion as shown in Fig. 6.

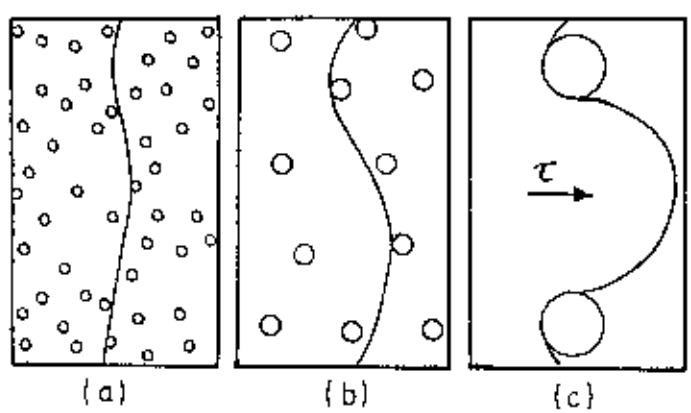

Fig. 6. Interaction between dislocation and foreign atoms in various states of dispersion.

For a homogenous solid solution case (a) applies where the distance between neighbouring stress centres $\Lambda \sim b/c^{1/3}$ is smaller than the minimum radius of curvature R of the dislocation under stress $R \sim \mu b/\tau_j$

Cotrell (1953) has calculated that a non-vanishing average stress τ_c is felt only by a dislocation segment of finite length L, and is of the magnitude:

$$\tau_c = \tau_j (\Lambda/L)^{1/2} \sim \mu |\delta|^{4/3} c$$

L is estimated as the minimum loop length whose statistical amplitude due to curvature 1/R is equal to A, the distance between obstacles. τ_c is independent of temperature.

(b) Weak Localized Forces

Fleischer (1961, 1963) showed by assumption that an individual solute atom interacts with a dislocation in the same way as a volume b^3 with a shear modulus differing from that of a matrix $\Lambda\mu$. Such elastically hard or soft spots in the matrix are felt by screw as well as edge dislocations. This interaction is called 'dielastic', as it is induced by the dislocation. Kocks (1966), Foreman and Makin (1966), Naborro (1967) conclude that the localized interaction with solute atoms immediately above and below the slip plane always predominates. However, the elastic interactions are not localized in the sense that their interaction range is small compared to the distance between solute atoms, except for very small solute concentrations.

(c) Core Interaction

Friedel (1956) has shown that at low temperatures the dislocation will assume a zigzag shape despite an increase in line energy in order that some solute atoms lie in their energetically most favourable positions in the dislocation core.

(d) Local Order Friction

A non-ideal solution may locally establish short range order or solute clustering, depending on the sign of energy mixing, Fisher (1954). If a dislocation moves over its slip plane through this alloy, favourable bonds will be replaced by less favourable ones. The binding energy across the slip plane will be decreased by Γ ergs/cm^2 and a stress τ_c is needed to drive the dislocation through the crystal.

$$\tau_c = \Gamma / b$$

This friction is independent of temperature below the diffusion range and depends quadratically on concentration for small 'c' Flinn (1958).

Irvine and Pickering (1963) showed that the effect of matrix composition on yield strength contributed by the elements like carbon, nitrogen, manganese and silicon is relatively small. However, manganese exerts a large effect on strength by depressing the transformation temperature which affects grain size and degree of precipitation as well as increasing dislocation density in ferrite. Manganese is usually limited to 1.5 to 1.7% to avoid too much depression of the transformation temperature and thus bainite formation which can lead to an embrittlement. All solutes, particularly the interstitial type, are detrimental to the impact-transition temperature. For any steel, a reduction in free nitrogen content causes a decrease in the impact transition temperature

and vice versa (MacKenzie, 1963; Smaill et al, 1976).

2.4 Solubility Product and Stoichiometric Ratio

Darken, Smith and Filer (1951) have shown that when aluminium nitride dissolves to form a solid solution of aluminium and nitrogen in austenite, the equilibrium constant or solubility product for the reaction;

AlN (solid) = Al + N (both in soln. in austenite)

can be represented by:

$$K_s = (\%\ Al)\ (\%\ N) \quad \ldots\ldots\ldots\ldots\ (2.14)$$

This equation states that K_s is equal to the product of the weight percentages of aluminium and nitrogen in solution in austenite in equilibrium with aluminium nitride, these being considered equivalent to the activities. They found that when the logarithm of K_s was plotted against the reciprocal of the absolute temperature, the resulting straight line, Fig. 7. could be represented by the equation:

$$\log K_s = -\frac{2400}{T} + 1.95 \quad \ldots\ldots\ldots\ldots\ (2.15)$$

where T is the temperature in degrees Kelvin ($^{o}C + 273$). This equation is valid only for the solution of AlN in austenite shows that the solubility increases with temperature. The temperature at which K_s is equal to the product of the "acid-soluble" nitrogen and the "acid-soluble" aliminium content of the steel is the temperature at which, at equilibrium all AlN will be dissolved.

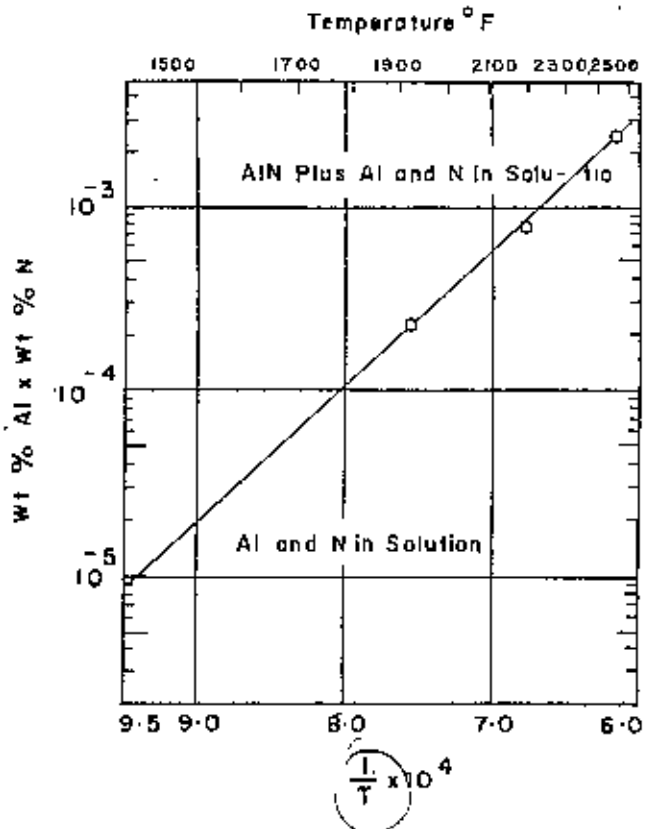

Fig. 7. Solubility Product of AlN in Austenite as a Function of Temperature.

Since the solubility product is the product of the concentrations of nitrogen and aluminium in solution in austenite in equilibrium with aluminium nitride, it can be expressed as follows:

$$K_s = (C_n - C_c)\ (C_{al} - \frac{27}{14}\ C_c) \quad \ldots\ldots\ldots (2.16)$$

where: C_n = weight % acid-soluble nitrogen

C_c = weight % nitrogen combined as AlN

C_{al} = weight % acid-soluble aluminium

$\frac{27}{14}\ C_c$ = weight % aluminium combined as AlN

K_s = Solubility Product at temperature ' concerned

Knowing C_n, C_{al}, and K_s, C_c can be calculated.

W.C. Leslie et at (1954) have shown that the equation (2.16) is modified by microsegregation of aluminium to give the "apparent" solubility product:

$$\log K_s = -\frac{6770}{T} + 1.033 \quad \ldots\ldots\ldots\ldots (2.17)$$

2.5 Metallurgical Design of Ferrite-Pearlite Steels

The metallurgical design of high strength, low-alloy steels with ferrite-pearlite structures require that compositional and microstructural parameters give the least increase in impact transition temperature per unit increase in yield strength, while maintaining an adequate level of weldability and formability.

Hardenability of a steel determines its weldability. Good weldability requires the steel to have a low hardenability which in turn is governed by the steel composition. Hardenability can be described by an empirical formula which defines

carbon equivalent (CE) value and takes account of the important elements which are known to affect hardenability. The formula most frequently use is:

$$CE = C + \frac{Mn}{6} + \frac{Cr + Mo + V}{5} + \frac{Ni + Cu}{15}$$

An arbitrary CE value of 0.41 is specified, above which welding may be hazardous. This equation emphasised that if manganese content is high, then low carbon content is essential.

The formability of ferrite-pearlite steels is affected by flow stress, work hardening rate, maximum uniform ductility prior to plastic instability and the total ductility at fracture. For good formability, the first two properties should be low while the last two should be high.

Pearlite and refining the interlamellar spacing of pearlite increases both the flow stress and work-hardening rate but reduce ductility (Gladman et al, 1970). Refining the ferrite grain size cannot offset the detrimental effect of pearlite but grain refinement is beneficial in terms of total ductility at fracture.

Non-metallic inclusions reduce the total ductility (Gurland and Plateau, 1963; McClintock, 1968), elongated inclusions are particularly detrimental to transverse ductility and upper shelf energy. Significant improvements in transverse ductility and upper shelf energy have been made in both plate and strip by reducing the volume fraction of inclusions or by inclusion shape control. Inclusion shape is modified by additing elements such as titanium, zirconium or rare earths to replace the elongated inclusions by spherical ones which may slightly reduce longitudinal ductility, but significant increases in both long-transverse and through thickness ductility occur.

Therefore, for good formability carbon and sulphur content should be low and the non-metallic inclusions should be uniformly distributed and shape-controlled.

Chapter 3

EXPERIMENTAL PROCEDURES

Chapter 3

EXPERIMENTAL PROCEDURES

3.1 Materials and Specimen Preparation

Plain carbon steel manufactured in the Chittagong Steel Mills Ltd., was taken as the base material. The composition is given in Table 1. Half of this steel was kept aside for further experiment and comparative study. The other half was used as raw material to manufacture aluminium alloyed steel.

Aluminium alloyed steel was made in an air induction furnace (35 lb. melt). The aluminium addition was made when the steel was sufficiently fluid. The melt was teemed at about 1600^{o}C immediately after aluminium addition and produced sound ingots. Piped ends of the ingots were discarded and scale removed.

Both plain carbon and aluminium steel were rolled down to 16 mm rod, after reheating at 1100^{o}C for half an hour. Standard tensile specimens with a nominal diameter and a minimum parallel length of 3.99 mm and 22 mm respectively were machined from each of the rods. Standard Charpy V-notch specimens were also prepared from the remaining portion of the rods.

3.2 Measurement of Prior Austenite Grains

In order to compare the properties of both steels without any undue complications, the steels were heat treated to a temperature which would give the same austenite grain size. A study was therefore made of the material so as to reveal the prior austenite grain boundaries at different austenitising temperatures. Isothermal Transformation Technique (Phillips and Chapman, 1963) was used to reveal the prior austenite grain boundaries.

3.2.1 Isothermal Transformation Technique

This technique is based on the rejection of ferrite or iron carbide at the austenitic grain boundaries, forming a complete or nearly complete network, in hypo eutectoid and hyper eutectoid steels, respectively. Steels with a carbon content remote from the eutectoid composition will reject, upon slowly cooling through the transformation range, either ferrite or cementite, depending upon the carbon content of the steel. The rejection of these constituents occurs largely at the prior austenite grain boundaries and, under appropriate conditions, the constituents may be made to form a network around the original grains.

The procedure used is as follows. The steel specimen were heated to different austenitizing temperatures, i.e. 850°C to 1100°C with intervals of 50°C. They were held at these temperatures for one hour. After one hour the specimens were transferred to a furnace at a lower temperature where ferrite rejection just takes place. This temperature was determined by trial and error and was found to be 760°C and 660°C for the plain carbon and aluminium alloyed steels, respectively. The specimens of plain carbon steel and aluminium alloyed steel are held at the above temperature for 15 minutes and 10 minutes respectively. The specimens were then quenched in water at room temperature.

The mean linear intercept method (Bepari, 1978) was employed to measure the austenite grain sizes. The specimens were sectioned, polished and etched, and placed under a Leitz optical microscope. The eyepiece of the microscope was provided with rectangular and circular cross-hairs. The length of the cross-hairs at different magnifications was determined by means of a stage micrometer. The number of grain boundaries intercepting the line of known length were counted. The magnification was so chosen that the maximum number of grains were intercepted by the line. About 500 intercepts were counted for each specimen. The grain size was determined by the relation:

$$\text{Grain Size} = \frac{\text{Length of Line}}{\text{Average Number of Intercepts}}$$

3.3 Determination of Heat-Treatment Temperature

The heat-treatment temperature was determined by a careful examination of the austenite grain sizes. A common austenite grain size of 55 microns was chosen, Fig. 8 and therefore the corresponding heat-treatment temperatures of 880°C and 1090°C for plain carbon steel and aluminium alloyed steel, respectively were obtained.

3.4 Heat-Treatment of Specimens

The heat-treatment of specimens was carried out in a Centorr Series 14 High Vacuum High Temperature and Controlled Atmosphere Electric Furnace by programmed operation

The operating principle of the furnace is as follows. The hot zone of the furnace is heated by means of a 25 KVA electrical resistance heating element. A SCR phase firing circuit continuously modulates the AC power input to the

furnace. The power input to the heating element is controlled by controlling the conduction angle of AC power flowing through the element. A sensor/transducer is used to sense the hot zone temperature.

Programmed operation is carried out by means of a Leeds & Northrup TRENDTRAK Programmer. A programme curve is drawn on a programme disc. A servo-driven photo-cell traces the programme curve. A signal is sent to the controller which in turn controls the current flowing to the heating element.

The specimens were suspended at the centre of the cylindrical heating element. The thermocouple was placed so that it accurately sensed the specimen temperature.

The specimens were heated in a gentle stream of helium gas at a pressure of 2 psig. They were held at the predetermined heat-treatment temperature for 30 minutes before cooling down to room temperature at four different cooling rates, namely; 110°C/min ; 40°C/min ; 12°C/min ; and 4°C/min. The heat-treatment schedule is shown in Fig. .

3.5 Mechanical Testing of Tensile and Charpy Specimens

3.5.1 Tensile Test

The heat-treated tensile specimens were tested with a Terco tensile testing machine to obtain data on yield strength, ultimate tensile strength, % elongation and % reduction in area. A travelling microscope was used to measure the maximum gauge length and minimum diameter after fracture of each specimen. The above values were calculated from the test results.

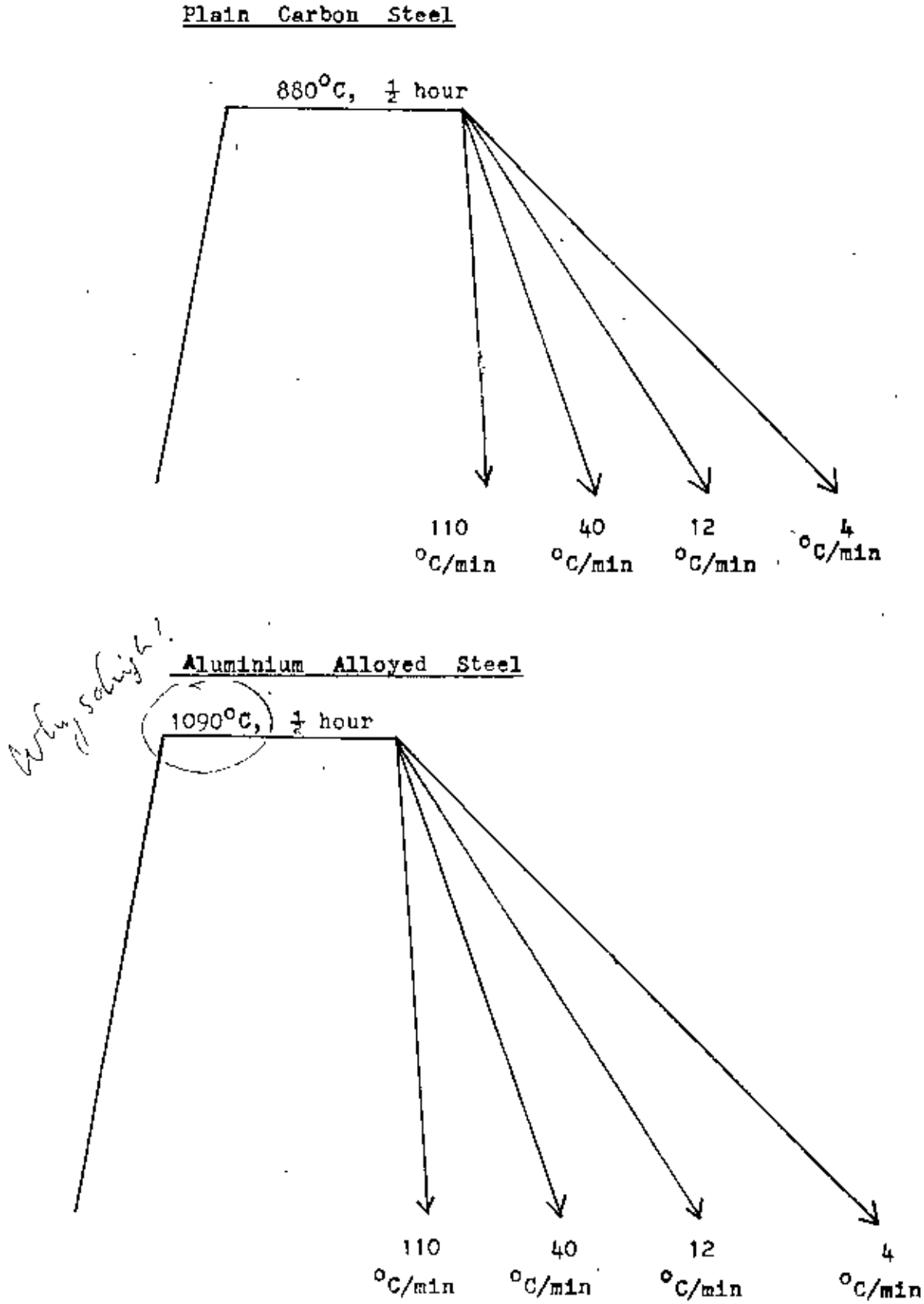

Fig. 22 Heat Treatment Schedule

3.5.2 Charpy V-Notch Test

The heat-treated charpy V-notch specimens were tested by means of a Sonntag Universal Impact Testing machine with a range of 0 - 240 ft. lbs. The specimens of each cooling rate were tested at temperatures of $0^{o}C$, $30^{o}C$, $100^{o}C$ and $200^{o}C$.

The specimens from each cooling rate were heated for ten minutes at each of the above temperatures. They were immediately transferred from the oven to the impact testing machine and tested. The results from the test were plotted in a curve and the impact transition temperature and upper shelf energy were determined.

3.6 Determination of Ferrite Grain Size and Hall-Petch Plot

Samples from the tensile specimens were taken and were mounted, ground, polished upto gamma alumina powder and then etched in 5% nital solution.

The measurement of ferrite grain size was carried out by the mean linear intercept method. As the microstructure was two phases, i.e. ferrite and pearlite, assessment of ferrite grain size had to be done in two stages. First, the fictitious ferrite grain size was measured. Only the grain boundaries of ferrite were counted, the pearlite between two ferrite grains was considered a common grain boundary. Next, the volume fraction of pearlite was estimated visually.

If the fictitious ferrite grain size is '$\overline{L}$' and the volume fraction of pearlite is 'v', then the true ferrite grain size 'd' is obtained by the following expression:

$$d = \overline{L} \quad (1 - v)$$

Hall-Petch plots of yield strength vs. $d^{-\frac{1}{2}}$ for both Stell I and Steel II were drawn to obtain an idea of how yield strength varied with the ferrite grain size.

Chapter 4

EXPERIMENTAL RESULTS

Chapter 4

EXPERIMENTAL RESULTS

4.1 Prior-Austenite Grain Size

The prior austenite grain of the steels were effectively revealed by the isothermal transformation technique as shown in Fig. 13 and 14. The size of the grains were determined by the mean linear intercept method. The grain sizes obtained are listed in Tables 2 and 3 and plotted against the austenitizing temperature in Fig. 8.

4.2 Heat-Treatment Temperature

The heat-treatment temperature was determined from an examination of the austenite grain size in Fig. 8. The criterion was such that the steels had the same austenite grain size and the temperatures were such that an appreciable proportion of the solute elements had gone into solid solution. This is indicated by a steep rise in the austenite grain size in the aluminium alloyed steel.

A common austenite grain size of 55 μm was chosen to fit that criterion and the corresponding heat treatment temperatures of 880°C and 1090°C were determined for plain carbon and aluminium alloyed steels, respectively.

The grain size of Si adjust. @ soaking time. What time was taken

4.3 Optical Microscopy

Both the steels gave a ferritic-pearlitic structure at all cooling rates. In Steel I, Plain Carbon Steel regular ferrite-pearlite was observed at all cooling rates, Fig. 15-18. Table 4 shows that pearlite content in the plain carbon steel does not vary greatly. The average volumetric percentage of pearlite in plain carbon steel is 24 %.

In Steel II, Aluminium Alloyed Steel the pearlite content varies greately, Table 5. The average volumetric percentage of pearlite in this stell is 59 %. At the slow cooling rates of $4^{o}$and 12^{o}C per minute fairly regular ferrite-pearlite structure was observed. But at the fast cooling rate of 40^{o}C and 110^{o}C per minute ferritic network around the pearlite was observed, Fig. 20. At the cooling rate of 40^{o}C per minute a few areas showed regular ferrite-pearlite structure. At the slow cooling rate of 4^{o}C per minute one area showed very fine grains, Fig. 21. This is due to the segregation effect of manganese.

4.4 Ferrite Grain Size and Hall-Petch Plots

The data from the tensile testing together with the pearlite volume fraction and the true ferrite grain sizes of the steels are presented in Tables 4 and 5. The mean ferrite grain size for both steels at the four cooling rates are presented in Fig. 9. Using the values of yield strength and $d^{-\frac{1}{2}}$, a Hall-Petch relationship is plotted in Fig. 10.

4.5 Impact Test

How did you find the transition temp. and shelf energy?

The impact energy absorbed at different temperatures is presented in Tables 6 to 13 and plotted in Fig. 11 and 12. The impact transition temperatures of the steels at each cooling rate was taken from the curves corresponding to 20 ft. lb. impact energy and listed in Tables 14 and 15. The upper shelf energy for each steel at each cooling rate is also presented in Tables 14 and 15.

Table 1

Composition

Steel	Composition, %				
	C	Mn	Si	Al	N
I Plain Carbon Steel	0.20	0.37	0.30	-	0.0034
II Aluminium Alloyed Steel	0.40	0.79	0.40	0.243	0.0044

Table 2

Austenite Grain Size

Steel I, Plain Carbon Steel

Temperature °C	Austenite Grain Size (um)
850	48
900	65
950	84
1000	91
1050	99
1100	117

Table 3

Austenite Grain Size

Steel II, Aluminium-Alloyed Steel

Temperature °C	Austenite Grain Size (um)
850	-
900	24
950	27
1000	29
1050	33
1100	61
1150	94

Table 4

Plain Carbon Steel

Heat Treatment Temperature: 880°C

Cooling Rate °C/min.	Ferrite Grain Size 'd' (mm)	$d^{-\frac{1}{2}}$ $(mm)^{-\frac{1}{2}}$	Y.S. N/mm^2	U.T.S. N/mm^2	Elongation %	R of A %	Pearlite %
4	0.0382	5.12	280	580	18	44	20
	0.0367	5.22	290	619	16	46	20
12	0.0314	5.64	310	580	21	39	20
	0.0308	5.70	300	576	19	43	20
40	0.0249	6.34	320	540	35	60	25
	0.0249	6.34	320	560	33	61	25
110	0.0154	8.06	345	576	32	61	28
	0.0146	8.28	340	560	34	53	32

Table 5

Aluminium Alloyed Steel

Heat Treatment Temperature: 1090°C

Cooling Rate °C/min.	Ferrite Grain Size 'd' (mm)	$d^{-\frac{1}{2}}$ $(mm)^{-\frac{1}{2}}$	Y.S. N/mm^2	U.T.S. N/mm^2	Elongation %	R of A %	Pearlite %
4	0.0199	7.09	380	780	14	24	45
	0.0196	7.14	384	820	22	27	50
12	0.0149	8.19	400	780	15	38	50
	0.0149	8.19	400	860	16	38	50
40	0.0118	9.21	440	880	17	38	55
	0.0111	9.49	440	860	17	34	60
110	Non - polygonal		560	900	13	16	80
	ferrite - pearlite		528	900	14	21	80

Table 6

Impact Energy Absorbed

Steel I, Plain Carbon Steel

Cooling Rate: 4°C/min.

Temperature °C	Impact Energy Absorbed (ft. lb.)
0	12
30	49
100	108
200	132

Table 7

Impact Energy Absorbed

Steel I, Plain Carbon Steel

Cooling Rate: 12°C/min.

Temperature °C	Impact Energy Absorbed (ft. lb.)
0	12
30	64
100	130
200	138

Table 8

Impact Energy Absorbed

Steel I. Plain Carbon Steel

Cooling Rate: 40°C/min.

Temperature °C	Impact Energy Absorbed (ft. lb.)
0	19
30	77
100	136
200	149

Table 9

Impact Energy Absorbed

Steel I. Plain Carbon Steel

Cooling Rate: 110°C/min.

Temperature °C	Impact Energy Absorbed (ft. lb.)
0	22
30	103
100	142
200	156

Table 10

Impact Energy Absorbed

Steel II, Aluminium-Alloyed Steel

Cooling Rate: 4°C/min.

Temperature °C	Impact Energy Absorbed (ft. lb.)
0	14
30	15
100	30
200	32

Table 11

Impact Energy Absorbed

Steel II, Aluminium Alloyed Steel

Cooling Rate: 12°C/min.

Temperature °C	Impact Energy Absorbed (ft. lb.)
0	17
30	19
100	38
200	43

Table 12

Impact Energy Absorbed

Steel II, Aluminium Alloyed Steel

Cooling Rate: 40°C/min.

Temperature °C	Impact Energy Absorbed (ft. lb.)
0	19
30	21
100	40
200	46

Table 13

Impact Energy Absorbed

Steel II, Aluminium Alloyed Steel

Cooling Rate: 110°C/min.

Temperature °C	Impact Energy Absorbed (ft. lb.)
0	20
30	23
100	40
200	49

Table 14

Impact Properties

Steel I, Plain Carbon Steel

Cooling Rate °C/min.	Impact Transition Temperature °C	Upper Shelf Energy (ft.lb.)
4	7	132
12	5	138
40	2	149
110	0	156

Table 15

Impact Properties

Steel II, Aluminium Alloyed Steel

Cooling Rate °C/min	Impact Transition Temperature °C	Upper Shelf Energy (ft.lb.)
4	52	30
12	33	43
40	10	45
110	0	47

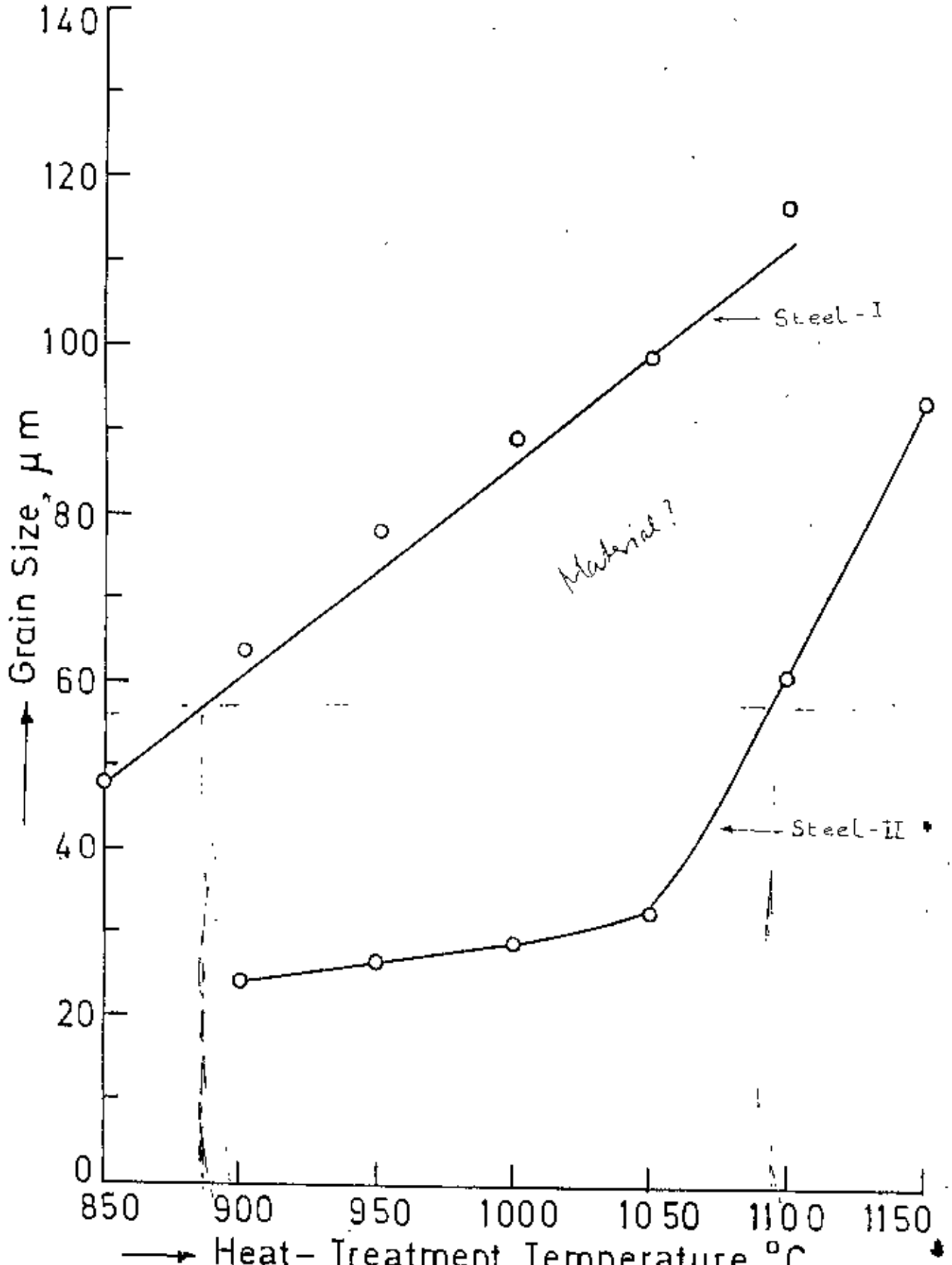

Fig. 8. Prior-Austenite Grain Size Vs. Heat Treatment Temperature.

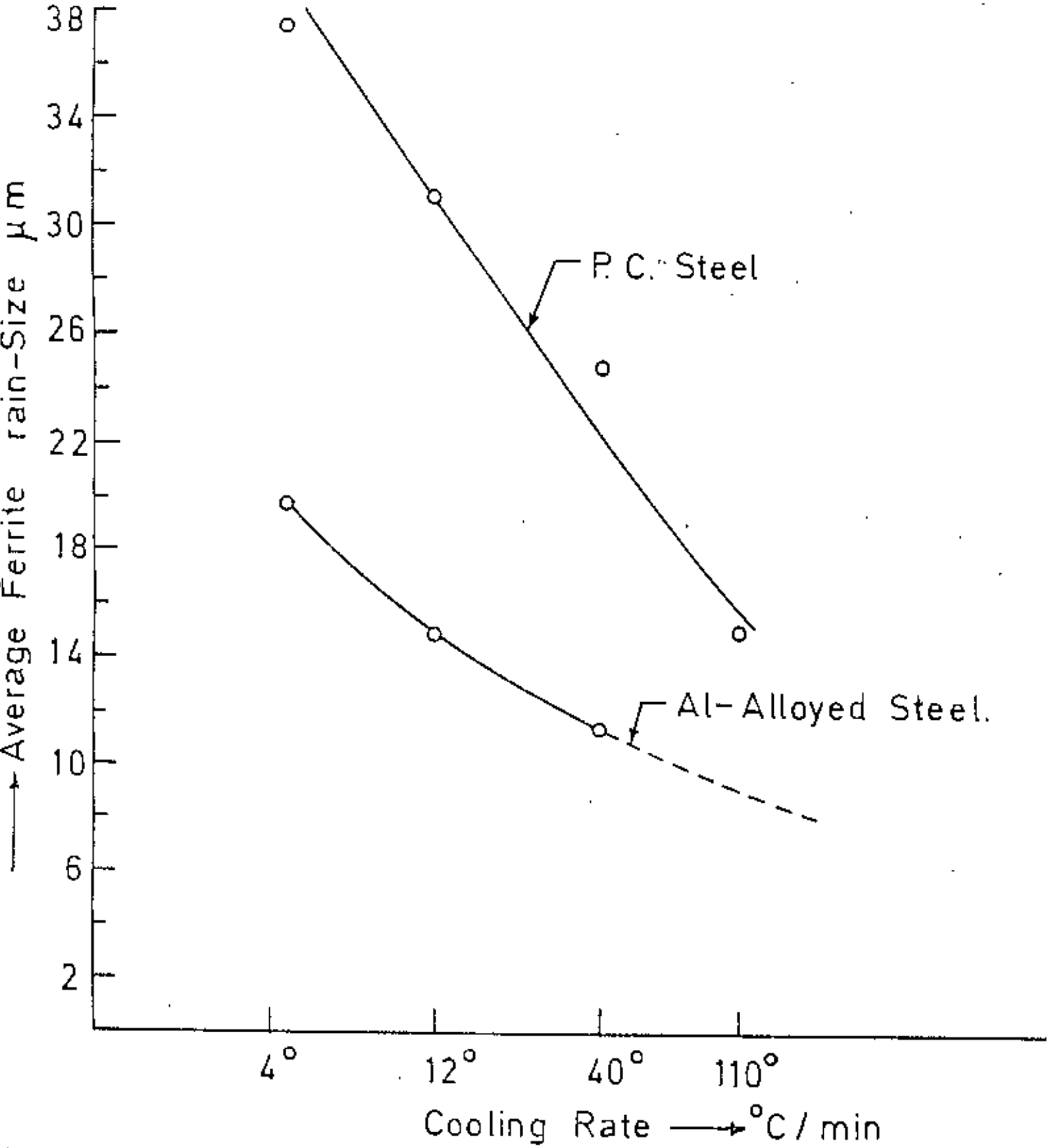

Fig. 9: Average Ferrite Grain Size Vs. Cooling Rate

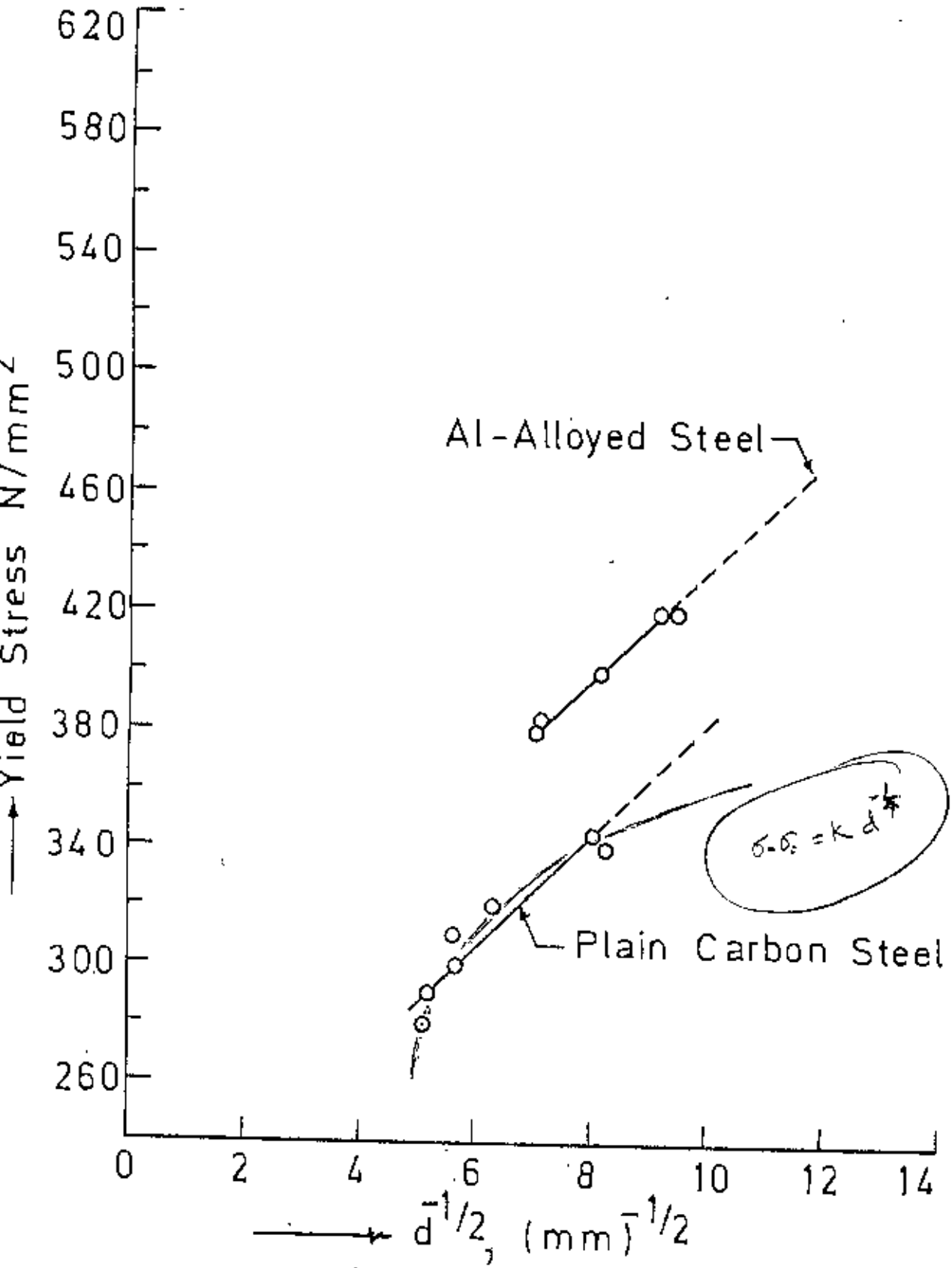

Fig.10. Hall-Petch Plots of Plain Carbon & Al Alloyed Steels.

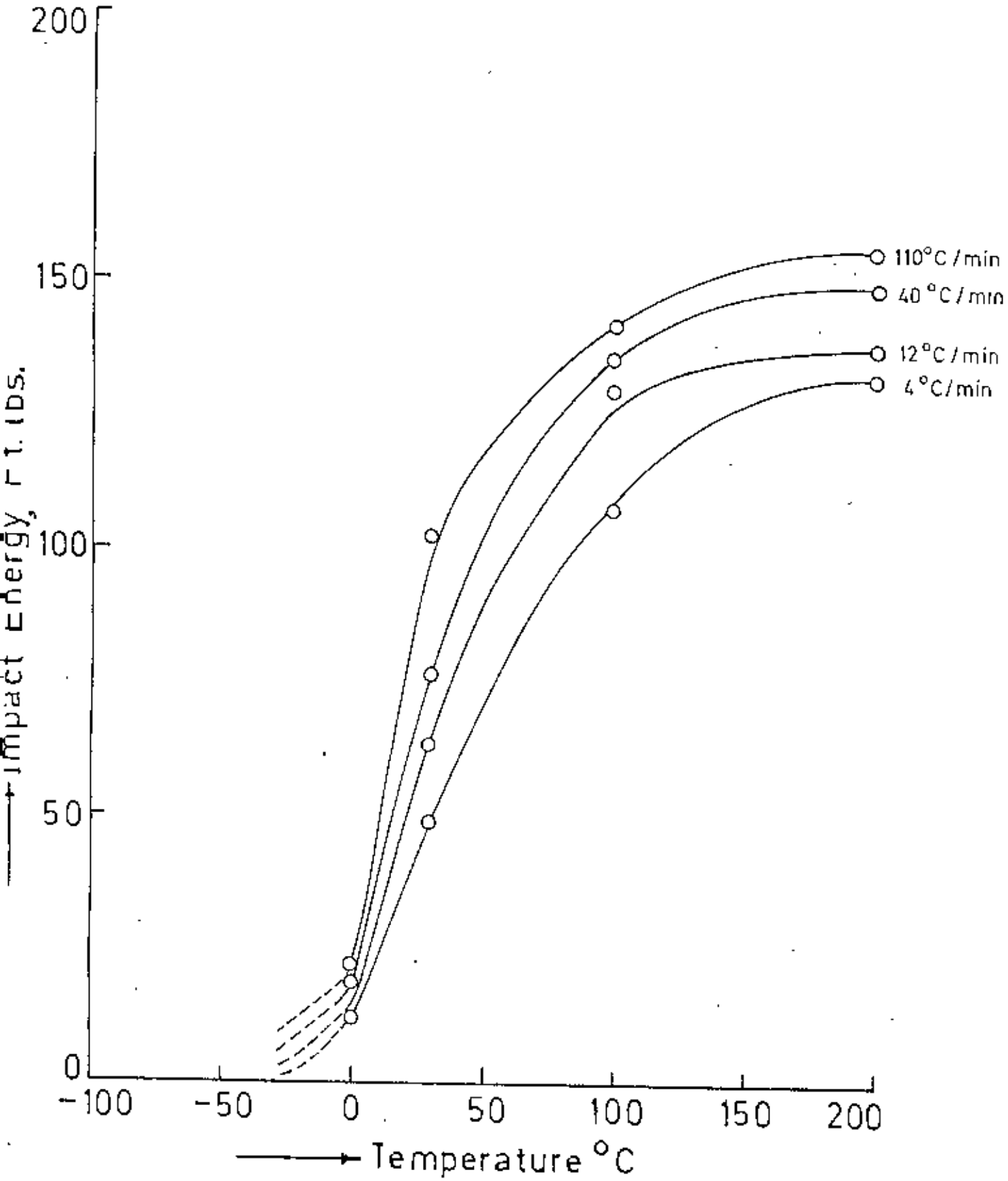

Fig. 11. Impact Energy Vs. Temperature, Plain Carbon Steel.

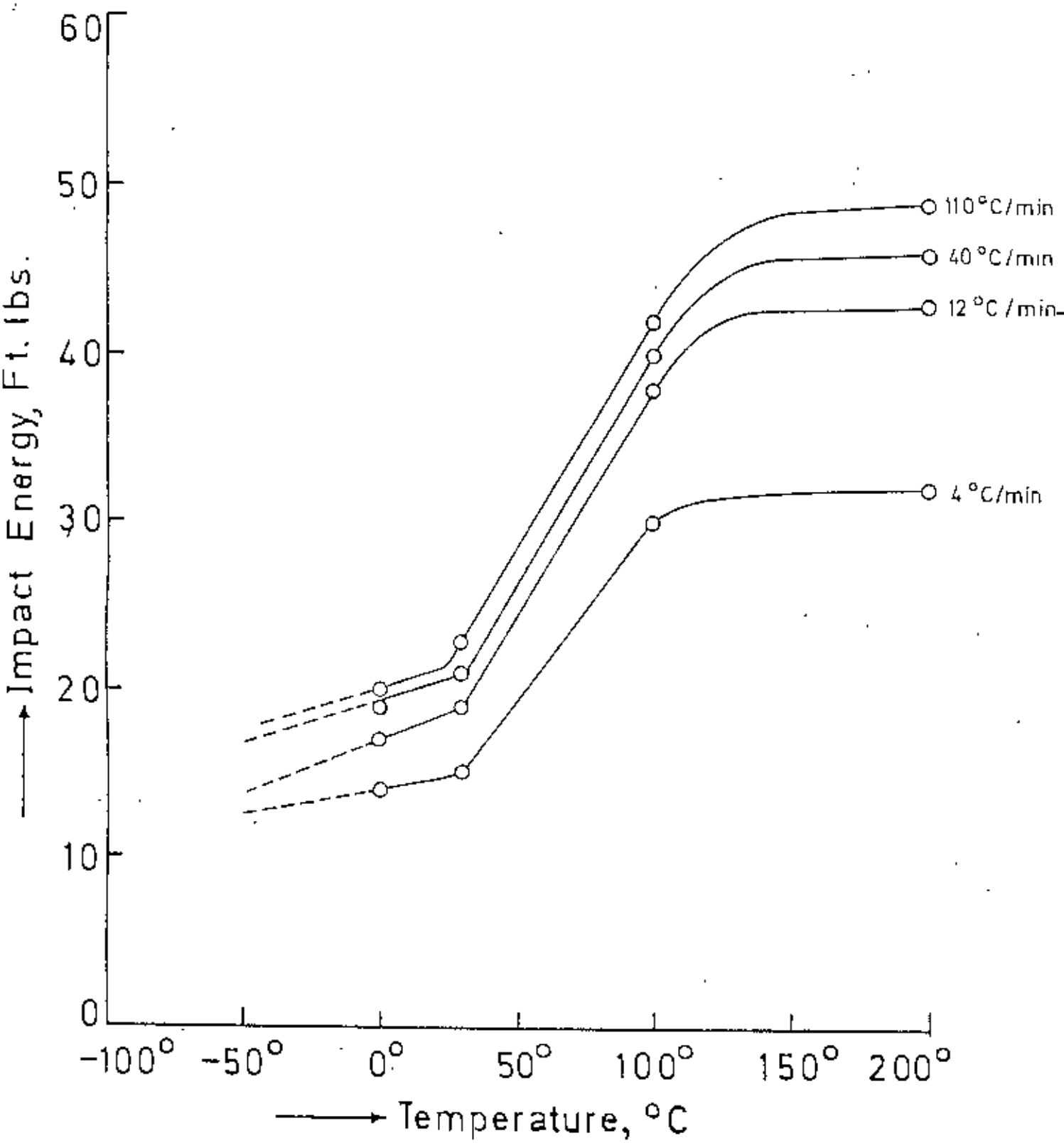

Fig. 12. Impact Energy Vs. Temperature, Al-alloyed Steel.

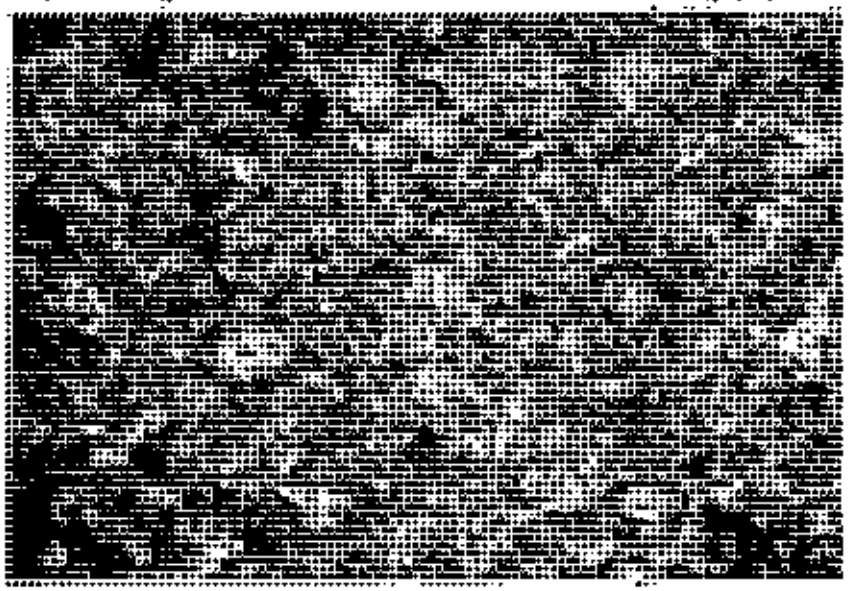

(a)

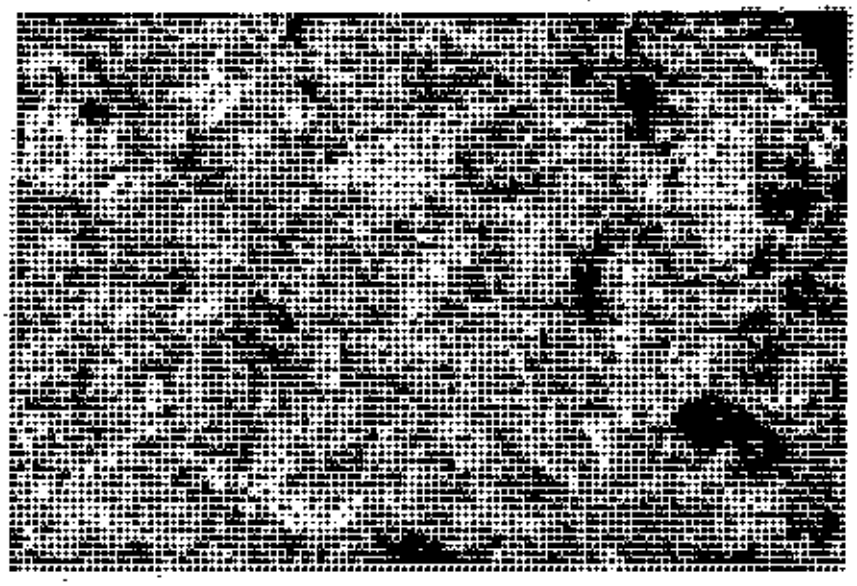

(b)

Fig. 13 Austenite Grain Size, Plain Carbon Steel, X120

(a) 900°C (b) 1050°C

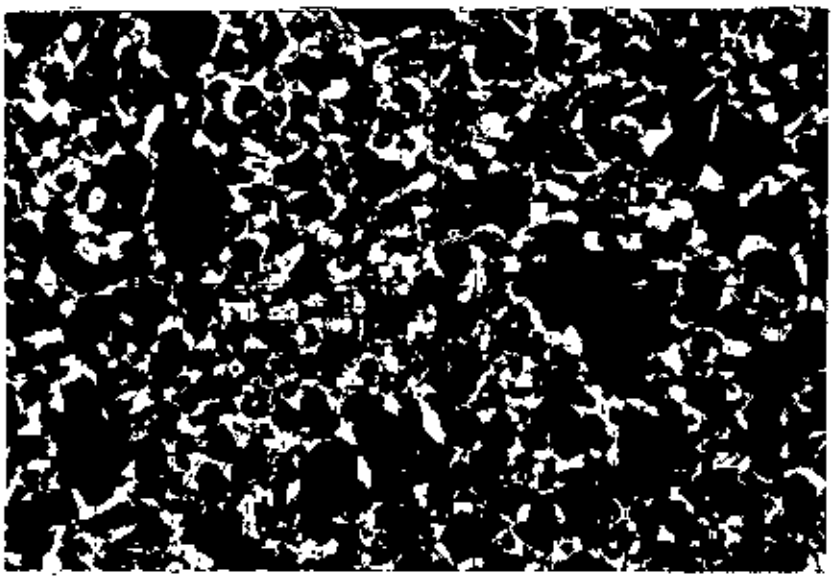

(a)

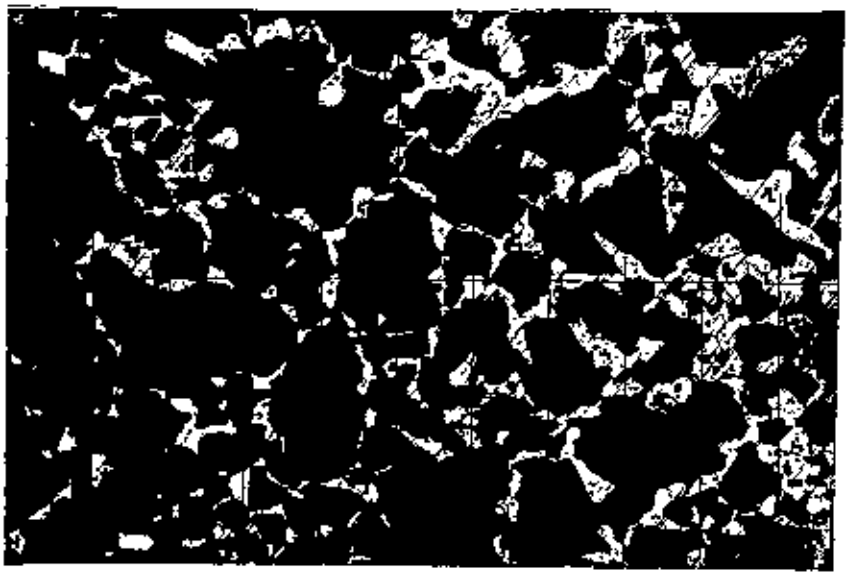

(b)

poor polishing

Fig. 14 Austenite Grain Size, Aluminium Alloyed Steel, X120
(a) 900°C (b) 1050°C

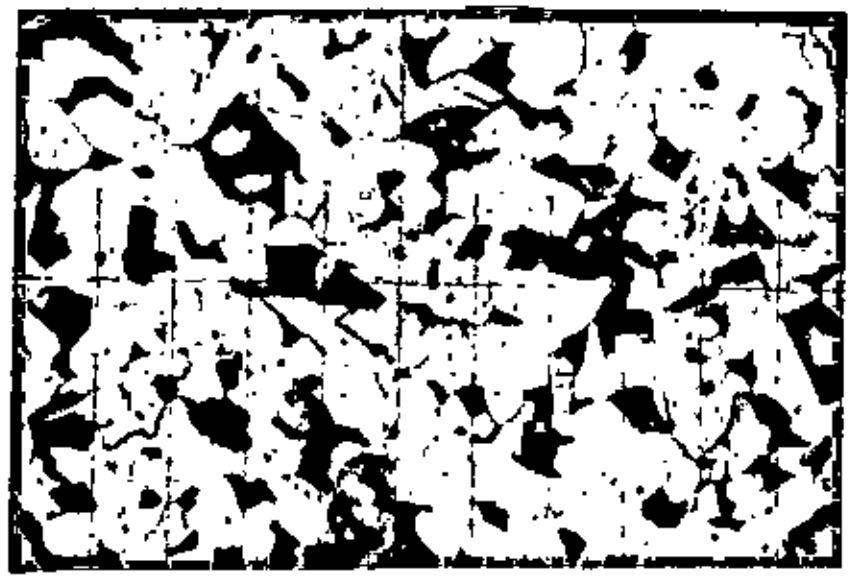

(a)

(b)

Fig. 15 Ferrite Grain Size, Plain Carbon Steel.
Cooling Rate: 4°C/min.
(a) X120 (b) X480

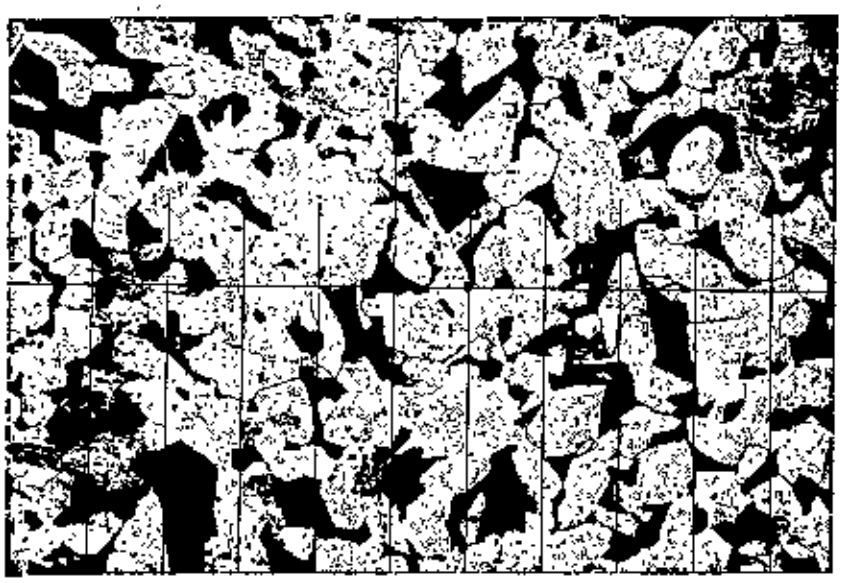

(a)

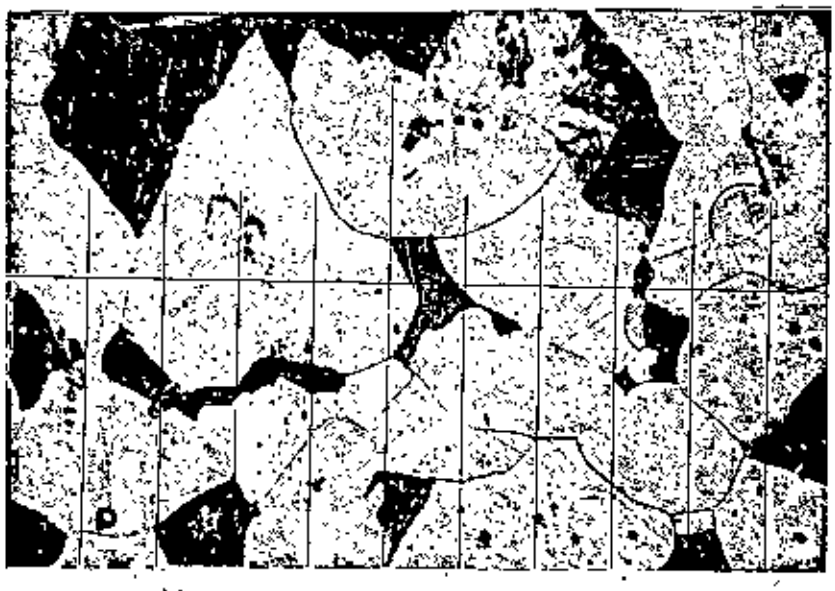

(b)

Fig. 16 Ferrite Grain Size, Plain Carbon Steel,
Cooling Rate: 12°C/min.
(a) X120 (b) X480

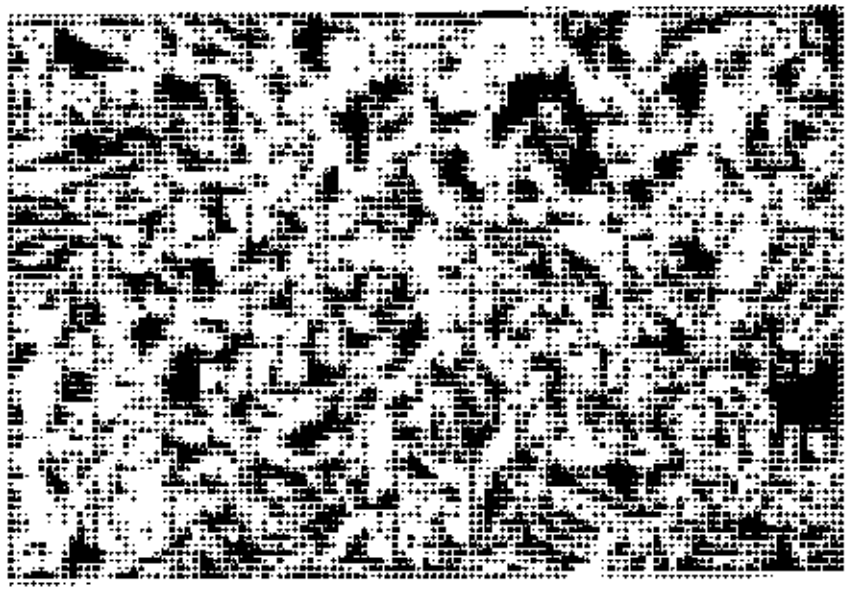

(a)

(b)

Fig. 17 Perrite Grain Size, Plain Carbon Steel.
Cooling Rate: 40°C/min.
(a) X120 (b) X480

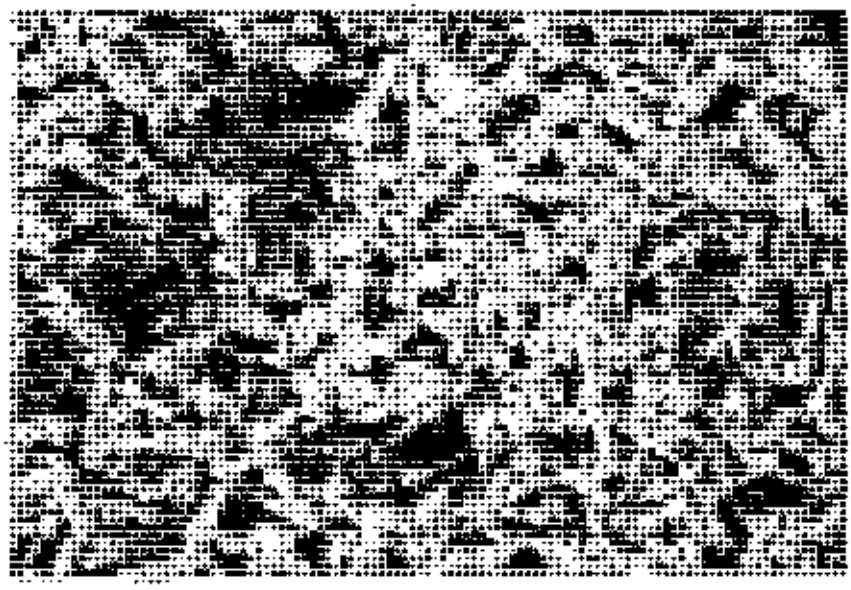

(a)

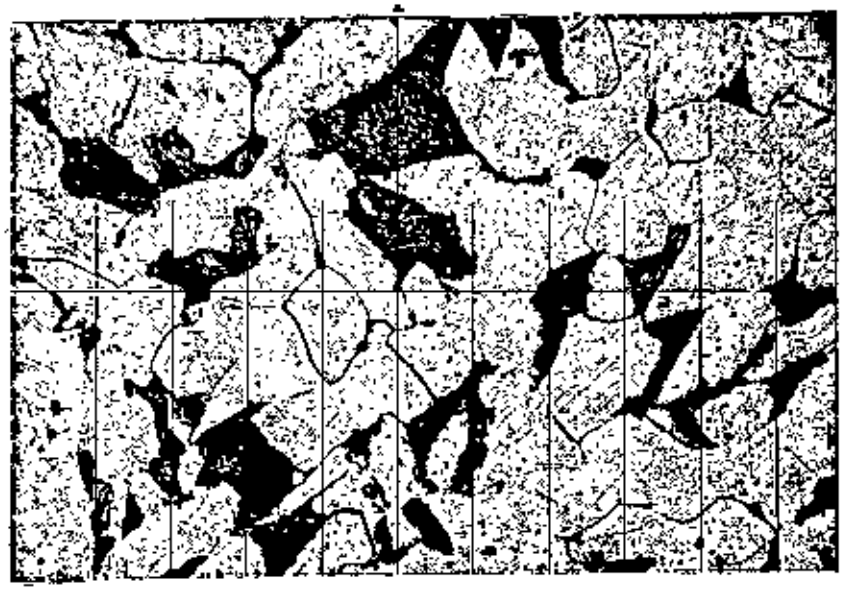

(b)

Fig. 18 Ferrite Grain Size, Plain Carbon Steel,
Cooling Rate: 110°C?min.
(a) X120 (b) X480

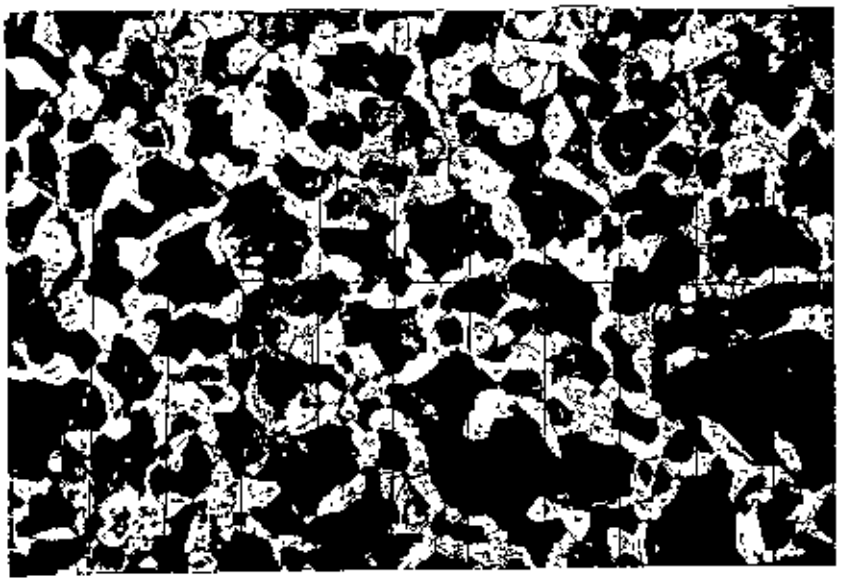

(a)

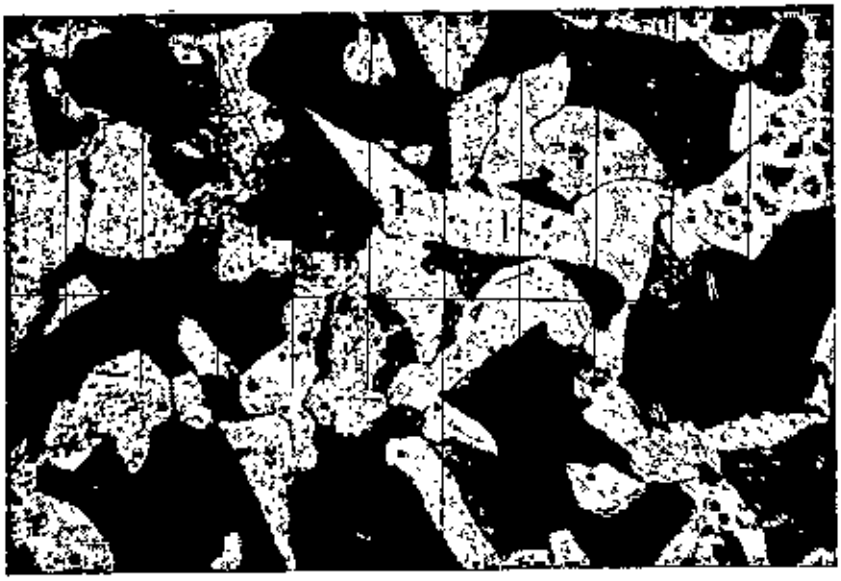

(b)

Fig. 19 Ferrite Grain Size, Aluminium Alloyed Steel, Cooling Rate: 4°C/min.
(a) X120 (b) X480.

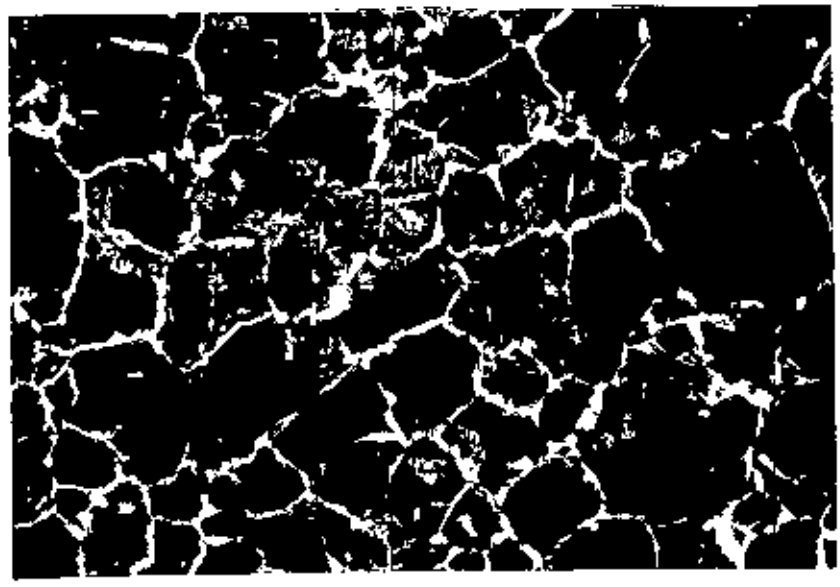

Fig. 20 Ferritic Network in Aluminium Alloyed Steel, Cooling Rate: 110°C/min., X 120.

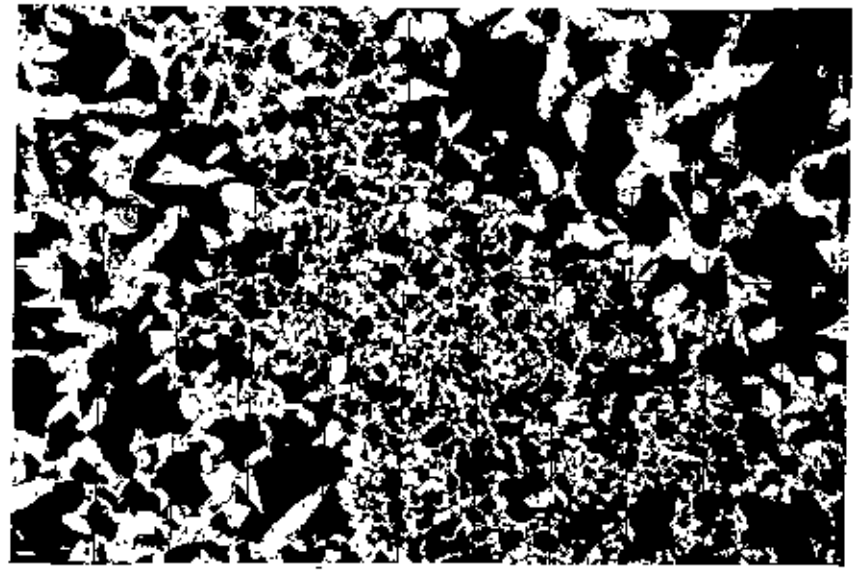

Fig. 21 Segregation Effect in Aluminium Alloyed Steel, X120.

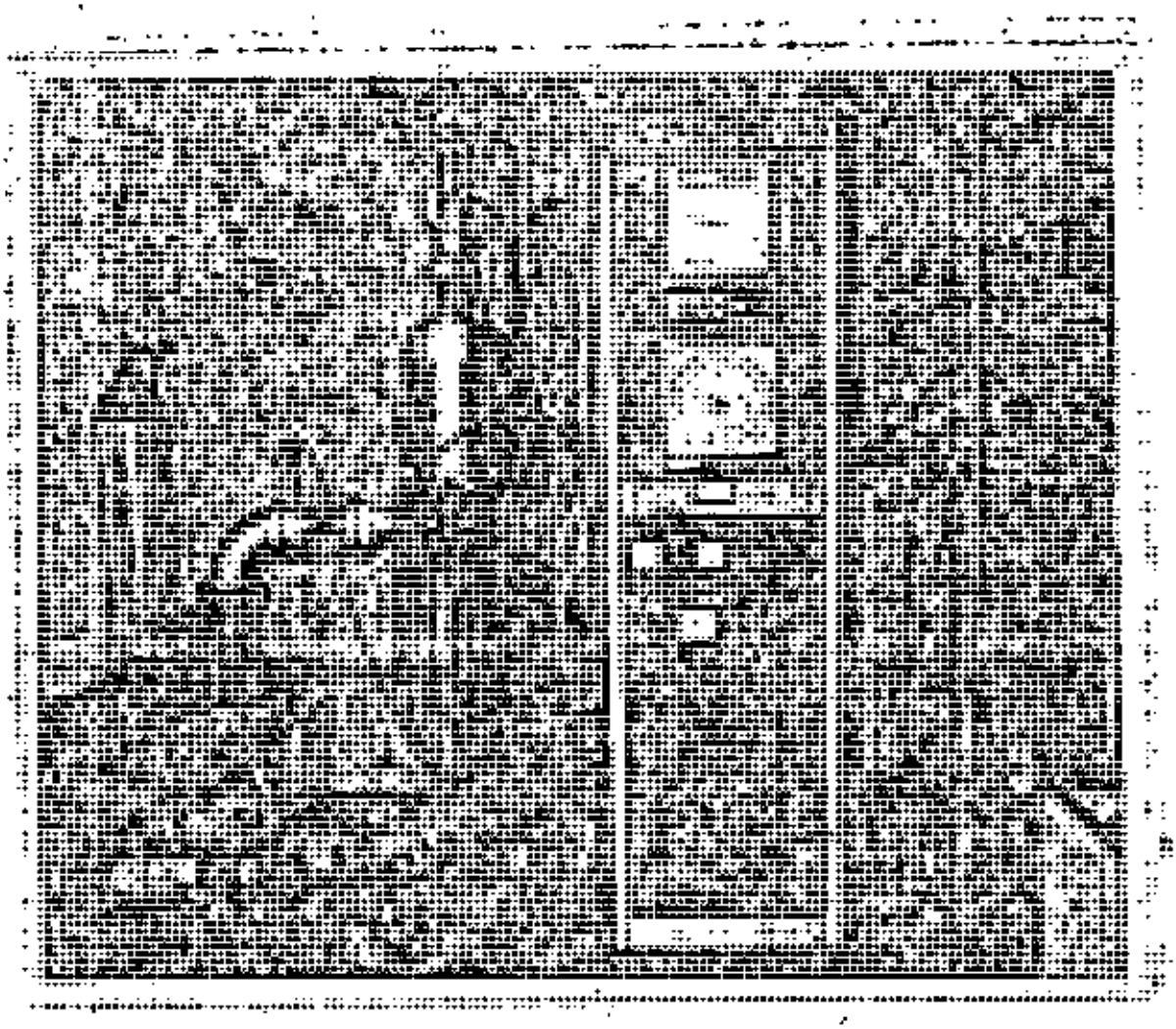

Fig. 23 Centorr High Temperature High Vacuum Controlled Atmosphere Electric Furnace

Chapter 5

DISCUSSION

Chapter 5

DISCUSSION

5.1 Making of Aluminium Alloyed Steel

Aluminium alloyed steel was manufactured in an air induction furnace. Aluminium addition was made just before pouring. Due to the lack of control over the process, the casting had to be repeated several times. Initially it was found that the steel was decarburized due to the high temperature of heating of the charge in presence of air in the furnace. Steps were taken to rectify this. The ingots for the next casting were found to contain extensive pipe formation. Finally, sound castings were obtained.

Decarburization of the steel was controlled by the addition of calculated amounts of high carbon steel. The steel thus manufactured was found to have retained an appreciable amount of carbon.

Extensive pipe formation was found to have taken place due to pouring in metal moulds. This was minimized by proper preheating of the ingot moulds. Good surface finish was obtained by coating the moulds with a mixture of graphite and water glass (sodium silicate, Na_2SiO_3).

Due to the unavailability of other means, file steel was used for the addition of carbon. Several drawbacks were found to have taken place. Addition of file steel not only increased the carbon content, but on chemical analysis it was

found to have greatly increased the manganese and silicon content in the steel manufactured, Table 1. There was no way of controlling this.

The aluminium addition in the steel was made just before pouring. The aluminium melted immediately and was stirred into the melt. It was seen that a large amount of aluminium was oxidised and from analysis it is found that only about 58 % of the original addition could be retained in the steel.

5.2 Prior-Austenite Grain Size

5.2.1 Isothermal Transformation Technique

This technique is based on the principle that ferrite or cementite precipitates preferentially at the austenite grain boundaries (Phillips and Chapman, 1963). Steels when brought down from austenitizing temperature and held for some time at some intercritical temperature, will reject ferrite or cementite at the prior austenite grain boundaries. The volume of this ferrite or cementite rejection is firstly a function of the inter-critical temperature and secondly a function of time at this temperature.

Of several techniques developed the most satisfactory is the recently developed oxidation technique (Niltawach, 1977) in observing prior-austenite grain boundaries. However due to lack of facilities this technique could not be used. For this reason the isothermal transformation technique was selected as it was the most appropriate, considering the facilities available.

The optimum inter-critical temperature at which a fine ferrite network around the prior austenite grains form was

obtained by trial and error. Since the holding time at this inter-critical temperature controls the thickness of the ferrite network, it too was determined in the same manner. However, an educated guess could be made from the $Fe-Fe_3C$ phase diagram to determine the holding temperature in the inter-critical range for plain carbon steels.

This technique worked well for Steel I, plain carbon steel at all temperatures. The effectiveness of this process in revealing the prior austenite grain boundaries is evident from Fig. 13.

Several problems were encountered with the determination of the inter-critical temperature and holding time in the case of Steel II, aluminium-alloyed steel as the $Fe-Fe_3C$ phase diagram is altered by the alloy additions and the extent of depression of the transformation region was not known. After much experimentation in the optimum inter-critical temperature for aluminium-alloyed steel was found to have been depressed by $100^{o}C$ (see 3.3.1) as compared to plain carbon steel. This is certainly due to the combined effect of aluminium together with high manganese, carbon and silicon content and the experiment had to be repeated many times before the holding time at the inter-critical temperature could be determined and reasonable ferritic network could be obtained. In determining the prior austenite grain size for Steel II, aluminium-alloyed steel, it was found that rejection of ferrite at the grain boundary did not take place as spontaneously during isothermal transformation as it did with plain carbon steel. It was seen that complete ferrite network was not obtained, Fig. 14. This clearly indicates that the presence of aluminium together with high manganese, silicon and carbon content retards the rejection of ferrite at the austenite boundaries.

5.2.2 Effect of Precipitates on the Prior Austenite Grain Size

From Fig. 8 it is evident that austenite grain size of plain carbon-steel, increases linearly with increasing temperature. This is due to the fact that second phase particles are not present in the steel. Therefore there is free migration of grain boundaries to attain the equilibrium grain size when the temperature is attained.

In the case of aluminium-alloyed steel, second phase particles of aluminium nitride, AlN are present. These second phase particles pin the austenite grain boundaries (see 2.3.1), thus causing the steels to retain a fine grain size which is unchanged during heating at successive high temperatures. It is seen from Fig. 8 that the prior austenite grain size of Steel II does not appreciably increase upto a temperature of about 1050°C. This indicates that aluminium nitride particles are effective upto 1050°C in this steel, exercising a pinning effect upto that temperature. Beyond 1050°C there is a sharp rise of prior austenite grain size with increasing temperature. It is reported by Bepari and Woodhead (1982), on heating undissolved aluminium nitride particles lose their effectiveness in inhibiting austenite grain growth at successive high temperatures due to their solution and coalescence. Thus in the present work as the austenitizing temperature exceeds 1050°C , solution and coalescence of aluminium nitride particles occur, causing accelerated grain growth.

5.3 Ferrite Grain Size and Hall-Petch Plot

The mean ferrite grain size of both plain carbon and aluminium alloyed steel at four different cooling rates is presented in Fig. 9. It is evident from this figure that although both the steels had originally started with a common austenite grain size, the subsequent ferrite grain size at the same cooling rate was not the same.

From Fig. 9 and Table 4 we see that in the case of plain carbon steel as the cooling rate increases the ferrite grain size 'd' decreases.

In aluminium-alloyed steel Fig. 9 and Table 5 show a finer ferrite grain size 'd' at all cooling rates. It is reported by Niltawach (1977) and Bepari (1981) that AlN precipitates do not have any effect on ferrite grain refinement because of its sluggish precipitation kinetics and as a result plain carbon and aluminium alloyed steel both show identical behaviour with respect to ferrite grain size. In the present work the finer ferrite grain size in Steel II is thus not due to the presence of aluminium nitride, but seems to be the combined effect of high carbon, manganese, silicon and Al in it.

Examination of the Hall-Petch plots, Fig. 10, of plain carbon and aluminium-alloyed steel shows a linear relationship for both. Plain carbon steel was used as the base steel with which strength and toughness of the aluminium-alloyed steel was compared.

Aluminium-alloyed steel at the cooling rate of $110^{\circ}C$ per minute showed an irregular ferritic network. Due to this it was not possible to determine the grain size. Examination of Fig. 10, will show that the Hall-Petch curve was therefore extended as a dotted line.

It has generally been accepted that when aluminium nitride has gone into solution it will not precipitate on cooling to give any precipitation strengthening (Bepari, 1978). On this basis it can be reasoned that the Hall-Petch plot of Steel II should be a straight line with the same slope as Steel I.

For plain carbon steel as the ferrite grain size decreases the yield strength increases. Similar behaviour is exhibited by aluminium-alloyed steel. However, aluminium-alloyed steel shows higher strength properties than plain carbon steel.

In Steel II, a part of aluminium is present as aluminium nitride and the rest is dissolved in ferrite. At the first sight of Fig. 10, the higher strength of Steel II seems to be due to the aluminium nitride precipitates. But it has been reported (Niltawach, 1977; Bepari & Woodhead, to be published) that aluminium nitride does not produce any precipitation strengthening effect due to its sluggish precipitation kinetics during cooling. In fact at slow cooling rates the formation of aluminium nitride, retards the strengthening process as it depletes the amount of soluble nitrogen which is itself a good strengthener. As the cooling rate increases, the precipitation kinetics of aluminium nitride becomes more unfavourable and this is accompanied by a corresponding increase in the residual soluble nitrogen. Thus the strength increases with faster cooling rate.

Table 5, shows that for aluminium-alloyed steel, the pearlite content increases with increasing cooling rate. It is known that pearlite upto 30 % has little or no effect on the yield strength. Beyond that the effect of pearlite on yield strength is quite appreciable. Since the pearlite content of aluminium-alloyed steel varies from 45 % to 80 % with cooling rate, the higher strength of this steel is largely due to the pearlite content.

In ferrite-pearlite steels manganese lowers the transformation temperature range. The transformation range becomes much narrower than for binary iron-iron carbide alloys. Due to this the ferrite grains have much less time for growth. This results in finer ferrite grains which give a higher yield

strength. Manganese has an affinity to remain in solution in ferrite. This causes a marked increase in the strength of the matrix. In steels containing a higher percentage of carbon and manganese, there is a possibility of Mn_3C formation. This carbide has a marked hardening effect. It is thus obvious that higher percentage of manganese present in aliminium-alloyed steel is also responsible for higher yield strength.

Silicon in steel also remains in solid solution in ferrite, thus strengthening the matrix. In Steel II, aluminium-alloyed steel this is one of the reasons why higher strength was obtained.

Aluminium dissolved in ferrite seems to contribute a considerable effect on yield strength. The higher yield strength of aluminium-alloyed steel than plain carbon steel is clearly due to the combined effect of free nitrogen, high manganese, carbon, silicon and aluminium dissolved in ferrite.

5.4 Impact Transition Temperature

The impact transition temperature (ITT) is a measure of the impact porperties of a material. The lower the impact transition temperature, the greater the toughness, therefore the better is the steel.

Fine ferrite grain size is the predominant factor which decreases the impact transition temperature. The finer the ferrite grain size the lower the ITT (equation 2.2). Increasing carbon content increases pearlite which in turn increases the impact transition temperature (equation 2.2). Increase in free nitrogen and silicon content also increases the ITT.

Table 14 shows that for plain carbon steel as the cooling rate increases the impact transition temperature decreases. This is due to the decrease in ferrite grain size. Table 4 however shows that for plain carbon steels when the cooling rate increase, the pearlite content increases but the variation of pearlite is not great. Increasing pearlite content raises the impact transition temperature. On the other hand increasing cooling rate decreases the ferrite grain size. Calculation shows that the beneficial effect of the finer ferrite grains on the impact transition temperature with increase in cooling rate is much more than the detrimental effect caused by increasing pearlite content. As a result the lower impact transition temperatures are obtained with the fast cooling rates.

Table 15 shows that for aluminium-alloyed steel too, as the cooling rate increases the impact transition temperature decreases. Aluminium-alloyed steel showed finer grain size than plain carbon steel. Finer ferrite grain size decreases the impact transition temperature. However Table 15 shows that aluminium-alloyed steel has a much higher impact transition temperature than plain carbon steel at all the cooling rates except 110^{o}C per minute whereas the reverse should be true considering the finer ferrite grain size. This can be explained in terms of the carbon, silicon and aluminium content.

Tables 1 and 5 show that the carbon content hence the amount of pearlite in aluminium-alloyed steel is much higher than that present in plain carbon steel. From equation 2.2 it is seen that this increasing pearlite content must have a large detrimental effect on the impact transition temperature. The high silicon content also tends to raise the impact transition temperature. Finally the steel contains aluminium, a part of which is present as aluminium nitride particles. The aluminium nitride particles increases the ITT (Bepari, 1981). The rest of the aluminium which is dissolved in ferrite also raises the impact transition temperature (Pickering et al).

The higher impact transition temperature in Steel II than in Steel I at these cooling rates is thus clearly the combined effect of pearlite, silicon, aluminium dissolved in ferrite and aluminium nitride.

At the fast cooling rate of 110°C per minute both aluminium alloyed steel and plain carbon steel showed the same impact transition temperatures. Since there is a difference in composition and the ferrite grain size of aluminium-alloyed steel could not be determined because of ferritic network around the pearlite, it is unwise to attempt an explanation.

Chapter 6

CONCLUSION AND FUTURE SUGGESTIONS

Chapter 6

CONCLUSION AND FUTURE SUGGESTIONS

6.1 Conclusions

i. In manufacturing steels with aluminium addition in the air induction melting furnace, only about 58 % of the aluminium added is retained in the steel. Therefore approximately 1.8 - 2 times the amount required should be added just before pouring.

ii. The isothermal transformation technique is a satisfactory method for revealing the prior austenite grain boundaries in plain carbon steels.

iii. The presence of aluminium together with high manganese, carbon and silicon in carbon steels retards the rejection of ferrite when the steel is held at a temperature in the inter-critical range.

iv. Increasing carbon and manganese content in hypoeutectoid steel produces fine ferrite grains.

v. The undissolved aluminium nitride particles are effective in austenite grain growth inhibition for the hypoeutectoid steel at temperatures up to 1050^{0}C.

vi. Increasing carbon and manganese content in hypoeutectoid steels increases the yield strength.

vii. Aluminium dissolved in ferrite [illegible] increases the yield strength of hypoeutectoid steel.

viii. The increase in pearlite content raises the impact transition temperature.

ix. Aluminium, either as aluminium nitride, or dissolved in ferrite also raises the impact transition temperature.

6.2 Future Suggestions

i. Free nitrogen content in the steels at each cooling rate should be determined in order to evaluate the separate effect of free and combined nitrogen on the strength and toughness.

ii. Steels that are used should have the same composition but with aluminium added.

iii. The shape, size and distribution of the precipitate particles should be studied by the means of electron microscopy in order to understand their effect on the mechanical properties better.

References

Ashby, M.F., 1964, Z.f. Metallk., 55, 5

Ashby, M.F., 1966, "Oxide Dispersion Strenthening", AIMME Conf., New York, p.143

Barr, W., 1950, "The Fracture of Metals", Institute of Metallurgists", p.117

Bepari, M.M.A., 1978, M.Met. Thesis, University of Sheffield, England.

Bepari, M.M.A., 1981, Ph.D. Thesis, University of Sheffield, England

Bepari, M.M.A. and Woodhead, J.H., 1982, Journal of the Institution of Engineers, Vol.10, No. 2.

Bepari, M.M.A. and Woodhead, J.H., to be published

Bepari, M.M.A., to be published.

Cahn, R.W., ed. "Physical Metallurgy", 2nd edition, 1977, North-Holland Publishing Co.

Cotrell, A.H., Hunter, C.S. and Nabarro, F.R.N., 1953, Phil. Mag. 44, p.106.

Darken, L.S., Smith, R.P., and Filer, E.W., 1951, "Solubility of Gaseous Nitrogen in Gamma Iron and the Effect of Alloying Constituents - Aluminium Nitride Precipitation", Trans. AIMME, 191, p.1174.

Erasmus, L.A., 1964, JISI, p.128.

Fisher, J.C., 1954, Acta. Met. 2, 9.

Friedel, 1956, "Physical Metallurgy", Cahn, R.W. ed.

Foreman, A.J.E. & Makin, M.J., 1966, Phil. Mag. 14, 131.

Fleischer, R.L., 1963, Acta. Met. II, 203.

Flinn, P.A., 1954, Acta. Met. 6, 631.

Gray, J.M., Webster, D. and Woodhead, J.H., 1965, JISI., 203, 312.

Gladman, T., 1966, Proc. Roy. Soc., Series A, 294, 298.

Gladman, T., "Effect of Aluminium Nitride on the Grain Coarsening Behaviour of Austenite"

Gladman, T., Dulieu, D. and McIvor, I.D., 1975, Microalloying 75 Symposium, Washington D.C., October, p.25.

Gladman, T., Holmes, B. and Pickering, F.B., 1970, JISI, 208, 173.

Gladman, T., McIvor, I.D. and Pickering, F.B., 1972, JISI, 210, 916

Gladman, T. and Woodhead, J.H., 1960, JISI, p.189.

Gladman, T. and Plateau, J., 1963, Trans. A.S.M., 56, 442

Hall, E.O., 1951, Proc. Phys. Soc., Series B, 64, 747.

Halliday, W.I., 1963, "Metallurgical Development in Carbon Steels", ISI Special Report No.81, p.65.

Haasen, P., 1959, Internal Stresses in Metals, G.M. Rassweiler and W.L.Grube, eds. (Elsevier Publ. Co., Amsterdam)p .205

Haasen, P., 1977, Physical Mettallurgy, 3rd. printing, R.W.Cahn ed., North Holland Pub. Co., p.1011.

Haque, E., Loretto, M.H., and Jones, I.P., 1975, "Supplementary Atomic Displacement Near Stacking Faults in Silicon" Proceedings of EMAG 75, Bistol Confce., England, p. 429.

Hillert, 1965. Gladman, T., 1966, Proc. Roy. Soc., Series A, 294, 298.

Irvine, K.J., Gladman, T., Orr, J. and Pickering, F.B., 1970 JISI, 208, 717.

Irvine, K.J. and Pickering, F.B., 1963, JISI, 201, 944.

Irvine, K.J., Pickering, F.B. and Gladman, T., 1967, JISI, 205, 161.

Kelly, A., and Nicholson, R.B., 1963, Progress in Materials Science, 10, No.3, New York (Macmillan).

Kocks, U.F., 1966, Phil. Mag., 13, 541.

Le Huy, H., Krishnadev, M.R., and Galibois, A.

Leslie, W.C., Rickett, R.L., Dotson, C.L. and Walton, C.S., 1954, "Trans. ASM, p.1470

Martin, J.W., "Precipitation Hardening", 1st ed.,1968, Pergamon Press.

McClintock, F.A., 1968, "Ductility" ASM Seminar Volume, Metals Park, Ohio, p.255.

McLean, D., 1957, "Grain Boundaries in Metals", London (Oxford University Press), p.241.

Morrison, W.B., and Woodhead, J.H., 1963, JISI, 201, 43

Mott, N.F. and Nabarro, F.R.N., 1940, Proc. Phys. Soc., 52, 86

Mott, N.F. and Nabarro, F.R.N., 1948, Rep. Bristol Conf. Strength of Solids, (Phys. Soc., London), p. 1

Nabarro, F.R.N., 1967, "Theory of Dislocations", Oxford Clarendon Press

Niltawach, S., 1977, Ph.D. Thesis, University of Sheffield

Orowan, E., 1948, Inst. of Metals Symposium on Internal Stresses in Metals and Alloys, p. 451.

Petch, N.J., 1953, JISI, 174, 25

Petch, N.J., 1959, Swampscott Conf., M.I.T. Press, p. 54

Phillips, R. and Chapman, J.A., 1963, "Metallurgical Developments in Carbon Steels", ISI Special Report No. 81,p. 60.

Pickering, F.B., 1975, Microalloying 75 Symposium, Washington D.C., October, p.3.

Pickering, F.B. and Gladman, T., 1963, ibid., p.10.

Schoeck, G. and Seegar, A., 1959, Acta. Met., 7, p. 469.

Wiester, H.J., Vogels, H.A. and Ulmer, H., 1959, Stahl und Eisen, 79, No. 16, 1120

Yagi, Y., Fukutsuka,T. and Ogawa, R., 1972, Trans. ISIJ, 12, p. 233.

Zener, 1949, Ref. Gladman, T., Proc. Roy. Soc., Series A, 294, 298.